Food Chemistry 501 (2026) 147358

Contents lists available at ScienceDirect

Food Chemistry

journal homepage: www.elsevier.com/locate/foodchem

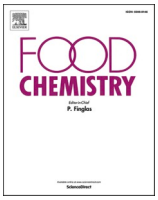

Encapsulation of C-phycocyanin in chitosan microparticles improves thermal and storage stability for use as a natural Food colorant

Paulo Vitor França Lemos [a,*,1], Nathalia Vieira Porphirio Veríssimo [b,c,**,1], Juliana Barone Teixeira [c], Henrique Rodrigues Marcelino [d], Guilherme Augusto Ferreira [e], Carolina Oliveira de Souza [f], Jania Betânia Alves da Silva [g], Thâmila Thalline Batista de Oliveira [h], Cristiano Luis Pinto de Oliveira [i], Marcia Carvalho de Abreu Fantini [i], Valéria de Carvalho Santos-Ebinuma [b]

[a] Institute of Pharmacy, Martin Luther University Halle-Wittenberg, Kurt-Mothes-Straße 3, 06120 Halle (Saale), Germany
[b] Department of Pharmaceutical Sciences, School of Pharmaceutical Sciences of Ribeirão Preto, São Paulo University, Ribeirão Preto, Brazil
[c] Department of Bioprocess and Biotechnology, School of Pharmaceutical Sciences, São Paulo State University (UNESP), Araraquara, Brazil
[d] Department of Medicine, Faculty of Pharmacy, Federal University of Bahia, Salvador, Brazil
[e] Department of Physical Chemistry, Institute of Chemistry, Federal University of Bahia, Salvador, Brazil
[f] Department of Bromatological Analysis, Faculty of Pharmacy, Federal University of Bahia, Salvador, Brazil
[g] Center for Exact and Technological Sciences, Federal University of Recôncavo da Bahia, Brazil
[h] SENAI CIMATEC University Center, Brazil
[i] Institute of Physics, University of São Paulo, São Paulo, Brazil

ARTICLE INFO

Keywords:
Microencapsulation
Blue colorant
Phycocyanobilin
Stability studies
Colorimetry
Fluorimetry

ABSTRACT

C-Phycocyanin (C-PC), a blue phycobiliprotein from microalgae, is a natural antioxidant and promising food colorant, but its use is limited by poor stability to heat, light, and pH. This study reports the encapsulation of C-PC in spray-dried chitosan (CHT) microparticles to improve its resilience. The microparticles displayed an average diameter of ~3.8 μm, positive ζ-potential (> + 24 mV), and encapsulation efficiency above 36 %. Spectroscopic and thermal analyses indicated the formation of a CHT–C-PC polyelectrolyte hydrogel network, while SAXS/USAXS revealed a heterogeneous porous architecture favoring C-PC retention. Encapsulation significantly enhanced C-PC stability under acidic (pH 2), alkaline (pH 10), and thermal stress, as well as during extended light/dark storage, reducing degradation markers such as color loss, turbidity, and spectral shifts. Stability was also preserved in gelatin matrices, where free C-PC rapidly degraded. Overall, chitosan microencapsulation effectively maintains C-PC integrity, enabling its application as a natural colorant in thermally processed and storage-demanding foods.

1. Introduction

The growing demand for natural, sustainable ingredients has boosted the interest of industry in C-phycocyanin (C-PC) due to its vibrant color, antioxidant activity, and natural origin. C-PC is increasingly used as a substitute for synthetic dyes, which face regulatory restrictions, such as the 2024 FDA-HHS ban on several petroleum-based colorants, over health concerns (U.S. Department of Agriculture and U.S. Food and Drug Administration, 2024). This underscores the need for stable natural alternatives compatible with industrial processing.

The global phycocyanin market is projected to exceed USD 230 million by 2030, with a compound annual growth rate (CAGR) surpassing 8 % (Grand View Research, 2023). Major international companies such as DIC Corporation (Japan, DIC Corporation, 2016), Sensient Technologies (USA, Sensient Technologies, 2025), GNT Group (Netherlands, GNT Group, 2019), and Naturex/Symrise (France,

* Corresponding author.
** Corresponding author at: Department of Pharmaceutical Sciences, School of Pharmaceutical Sciences of Ribeirão Preto, São Paulo University, Ribeirão Preto, Brazil.
E-mail addresses: paulo.lemos@pharmazie.uni-halle.de (P.V.F. Lemos), nathaliavieira@usp.br (N.V.P. Veríssimo).
[1] Shared co-first authorship.

https://doi.org/10.1016/j.foodchem.2025.147358
Received 5 September 2025; Received in revised form 16 November 2025; Accepted 28 November 2025
Available online 30 November 2025

Naturex, 2025) have invested heavily in the research, extraction, and purification of C-PC to meet the rising demand for clean-label and functional ingredients.

C-PC shows anti-inflammatory (Lemos et al., 2020; Shih et al., 2009), anti-allergic (Reddy & Subhashini, 2000), antioxidant (Mitra et al., 2015), and anti-tumor (Jiang et al., 2017) activities in vitro and in vivo. Its FDA-approved GRAS status (Chamorro-Cevallos et al., 2020, U.S. Food and Drug Administration (FDA), 2012), biological properties, and vibrant blue color make it a valuable natural additive for food and cosmetic formulations. Phycobiliproteins are water-soluble proteins that constitute 40 %–60 % of algal biomass (Galasso et al., 2019) and contain tetrapyrrole chromophores that absorb light between 470 and 660 nm (Glazer & Bryant, 1975). They are categorized as phycoerythrin (λ_{max} 565 nm), phycocyanin (λ_{max} 620 nm), and allophycocyanin (λ_{max} 650 nm) (Glazer & Bryant, 1975). C-phycocyanin consists of α (12–19 kDa) and β (14–21 kDa) subunits forming αβ monomers, which assemble into trimers and hexamers ($\alpha_6\beta_6$) as its functional structure (Eriksen, 2008).

Natural blue colorants are scarce and often unstable under heat, light, or acidic conditions, limiting their use in processed foods (Downham & Collins, 2000; Sigurdson et al., 2017). Therefore, synthetic dyes such as Brilliant Blue FCF have been widely used despite concerns over health effects and environmental persistence (Olas et al., 2021), prompting the FDA-HHS to initiate a phase-out of several petroleum-based dyes in 2024 (U.S. Food and Drug Administration (FDA), 2024). In contrast, C-PC is sustainably produced from microalgae using light, CO_2, and minimal water, aligning with global sustainability goals (Koyande et al., 2019; Moraes et al., 2020). Its dual role as a bioactive compound and stable natural colorant supports cleaner, fossil-free ingredient sourcing.

Despite its potential, the practical application of C-phycocyanin is hindered by its physicochemical instability. It is highly sensitive to pH, temperature, and ionic strength: denaturation occurs at pH <5.5 or > 8.0 (Zhang et al., 2022), and temperatures above 45 °C compromise its structural integrity and chromophore stability (Chaiklahan et al., 2021). This restricts its use in thermally processed foods, such as baked goods, gelatin-based desserts, and pasteurized beverages (Chaiklahan et al., 2021; Patil et al., 2006). Its instability under low pH also limits its incorporation into carbonated and fruit-based beverages (Esatbeyoglu et al., 2017), while its sensitivity to alkaline environments hampers its application in oral care and topical cosmetic products that require pH values above 8. Additionally, high ionic strength (e.g., >0.8 mEq NaCl) reduces its solubility via salting-out effects (Soni et al., 2020). These challenges underscore the need for strategies to stablize C-phycocyanin to enhance its functional stability in diverse applications.

Chitosan is a linear polysaccharide composed of β-(1 → 4)-linked D-glucosamine and *N*-acetyl-D-glucosamine units derived from the partial deacetylation of chitin. When amino groups are protonated in acidic conditions, the chitosan molecules become cationic. This lets it form electrostatic complexes and cohesive polyelectrolyte networks that trap biomolecules (Cheng et al., 2019; Sergeeva, Demina, & Sergeev, 2023). The semi-crystalline structure of chitosan, stabilized by intra- and intermolecular hydrogen bonding, contributes to the mechanical strength and permeability control of its matrices. Owing to these structural attributes, chitosan has shown high functionality as a wall material for the microencapsulation of colorants and proteins, effectively protecting them from heat and pH-induced degradation, as recently demonstrated by our group for fungal polyketide colorants (Galván et al., 2024).

Although there is an increasing interest in stabilizing C-PC, the number of publications on strategies to achieve it remains limited. Recent studies have explored chitosan-based encapsulation systems, including redox-sensitive nanoparticles (Cheng et al., 2019), water-soluble chitosan carriers (Gustiningtyas et al., 2020), sponges for controlled release (Sergeeva, Demina, & Sergeev, 2023), and protective nanoliposome coatings (Azari et al., 2023). Carboxylated chitosan has also shown efficacy in preserving C-PC under acidic conditions (Zhang et al., 2023). However, few reports describe polyelectrolyte gels that effectively enhance C-PC stability, and their structural mechanisms remain poorly understood.

Therefore, this study aimed to prepare C-phycocyanin microparticles using chitosan as wall material and to evaluate the colorimetric and fluorometric stability of C-PC under various pH levels, temperatures, and light exposure conditions. Structural characterization was also performed to elucidate the mechanisms by which this system preserves C-PC's properties. A detailed microstructural characterization was conducted for the first time on chitosan-based microparticles to elucidate the mechanisms by which this system enhances the stability of C-PC, expanding its potential applications in food, cosmetic, and pharmaceutical formulations.

2. Material and methods

2.1. Material

C-phycocyanin (C–PC) A620/A280 = 2.8 ± 0.1, above food (0.7) and cosmetic (1.5) grade purity (Patil et al., 2006; Payne et al., 2025), was purchased from Xian Pincredit Bio-Tech Co. Ltd., Chitosan (CHT) with a low molecular weight ranging from 50 to 190 kDa and a 90 % degree of deacetylation was purchased from Sigma-Aldrich (Scientific Laboratory Supplies, 2023). The other reagents, such as sodium tripolyphosphate (STPP) and acetic acid, were of analytical grade and were used as received.

2.2. Methods

2.2.1. C-phycocyanin Encapsulation

Microparticles based on CHT were prepared by spray-drying. A mass of 6 g of CHT was dissolved in 1 L of a 5 % (v v^{-1}) acetic acid solution (pH 3.57), and stirred magnetically at 700 rpm at 30 °C for 30 min. Subsequently, 3 g of C-PC were added to the solution before stirring under the same conditions. The resulting mixture was subjected to spray-drying to produce the CHT–C-PC system. To form CHT–STPP–C-PC, the same procedure was used, with the addition of 2.4 g of sodium tripolyphosphate after incorporating C-PC.

The mixture was dried in a spray-dryer MSD 0.5 (LabMaq, Ribeirão Preto/SP, Brazil) equipped with a standard 0.7-mm nozzle at 110 °C, an air flow rate of 20 L min^{-1}, an air feed of 0.21 L h^{-1}, and outlet temperature at 90 °C. For both mixtures with around 16.28 ± 0.02 mPa.s at 25 °C of viscosity, an atomization rate of 7 % and an aspiration rate of 100 % were used, enabling the drying of 150 mL of each solution per hour (Galván et al., 2024). We performed the same drying procedure on a C-PC solution (10 mg·mL^{-1}) as a control sample to depict the thermal effects of the spray drying process on this molecule (spray-dried C-PC).

2.2.2. Scanning Electron microscopy

Scanning electron microscopy (SEM) was performed using a TM 3000 microscope (Hitachi, Tokyo, Japan) to obtain and evaluate samples coated with a thin layer of gold. Micrographs were obtained at 100×, 500×, 1000×, and 2000× magnifications at an accelerating voltage of 15 kV. The lengths of microparticles (n = 20) were obtained using the software Image J and expressed as the mean ± standard deviation (Schneider et al., 2012).

2.2.3. Yield and encapsulation efficiency

The yield of the process was measured by a simple gravimetric procedure, according to eq. 1:

$$Yield(\%) = \frac{Remainder}{Initial} \times 100 \quad (1)$$

where the remainder consists of the weighted CHT–C-PC and CHT–STPP–C-PC dried powders, and the initial consists of the sum of the

nominal masses of CHT, C–PC, and STPP.

CHT–C-PC and CHT–STPP–C-PC were separately diluted to10 mg mL^{-1} in acetic acid solutions (5 %, v v^{-1}) using a magnetic stirrer (700 rpm, 30 °C) to a final volume of 50 mL, before centrifugation at 2800 ×*g* and 30 °C for10 min, The absorbances of the supernatants were obtained at λ 620 nm and λ 650 nm (Lambda 25, Perkin-Elmer).

C-PC concentration (mg mL^{-1}) of the supernatant of the encapsulation procedure was calculated using the simultaneous equations of Bennett and Bogorad (Bennett & Bogorad, 1973) and the absorbance at 620 and 650 nm following eq. 2:

$$C-PC(mg/mL) = \frac{A620 - 0.474 \times A650}{5.34} \quad (2)$$

Encapsulation efficiency (%EE) was calculated using eq. 3 (Yagoubi et al., 2018):

$$\%EE = \frac{(Nominal - Released)}{Nominal} \times 100 \quad (3)$$

where the Nominal corresponds to the total mass of C-phycocyanin weighed at the beginning of the encapsulation procedure, and the Released corresponds to the C–PC mass that remained in the supernatant of the C–PC encapsulation procedure, determined by eq. 2.

All experiments were conducted in three independent replicates and variables were expressed as mean ± standard deviation. Amber recipes were used and the glass apparatus were covered in all procedures to avoid the C–PC stress by light.

2.2.4. Phosphorous content

Phosphorus content was determined by visible spectrophotometry at 420 nm (Sechi & Marques, 2017). CHT–C-PC (100 mg) and CHT–STPP–C-PC (100 mg) were incinerated at 350 °C for 4 h. Ashes were mixed with distilled water, 1 mL HNO_3, and dissolved in 10 mL HCl and 1 mL HNO_3 (37 % and 65 % m/v), before they were heated to boiling. Final solutions were diluted to a final volume of 100 mL.

Aliquots (30 mL) were reacted with 10 mL ammonium vanadate–molybdate in 50 mL flasks and rested for 10 min before absorbance was measured (λ 420 nm; Perkin Elmer Lambda 25). A 1 mg mL^{-1} working standard solution was freshly prepared by diluting a 2 mg mL^{-1} phosphorus stock solution, and this working solution was used to construct the analytical curve (0.2–2.0 mg P; $R^2 = 0.9997$) using the same procedure. All analyses were done in triplicate, and results were expressed as mean values.

2.2.5. Zeta potential

The zeta potential (ζ) measurements were taken by a Zetasizer instrument (Nano ZS Series, Malvern Instruments, United Kingdom). Suspensions of samples CHT–C-PC and CHT–STPP–C-PC were separately prepared in deionized water (0.3 % m v^{-1}) and analyzed at 25 °C. All the experiments were conducted in triplicate and measurements were expressed as mean ± SD.

2.2.6. Fourier transform infrared spectroscopy coupled with attenuated total reflectance

The infrared spectra of spray-dried samples CHT, CHT–C-PC, CHT–STPP–C-PC, and spray-dried C-PC were obtained using an infrared spectrometer (FTIR 4100, Perkin-Elmer, Shelton, USA) equipped with an attenuated total reflectance (ATR) module containing a ZnSe crystal. The spectra were obtained at room temperature (25 °C) between 4000 and 400 cm^{-1}. A total of 64 scans with a resolution of 4 cm^{-1} were obtained. The obtained infrared spectra were normalized based on their highest absorbance using Origin Pro 8.5. We determined the C—H symmetric/C–H asymmetric, amide I/amide II, and CH_2 bending/CH_3 symmetric indices using ratios of absorbance intensities on eqs. 4, 5, and 6 (Zhang et al., 2021).

$$C-H\ symmetric \Big/ C-H\ asymmetric = \frac{A2932}{A2874} \quad (4)$$

$$Amide\ I \Big/ amide\ II = \frac{A1651}{A1545} \quad (5)$$

$$CH2\ bending \Big/ CH3\ symmetric = \frac{A1407}{A1382} \quad (6)$$

2.2.7. X-ray diffractometry

The diffractograms of spray-dried samples CHT, CHT–C-PC, CHT–STPP–C-PC, and spray-dried C-PC were obtained using X-ray diffraction (XRD, Rigaku X-ray diffractometer Miniflex 600, Japan), with CuKα radiation operating at 40 kV, 30 mA, a reading angle (2θ) of 5.0° to 80.0°, step mode 0.02, and a scan speed of 2° min^{-1}.

2.2.8. Differential scanning calorimetry

DSC measurements were performed on a differential scanning calorimeter (DSC) model Q20 (TA Instruments) previously calibrated according to the manufacturer's instructions. Approximately 3 mg of samples, including CHT, CHT–C-PC, CHT–STPP–C-PC, and spray-dried C-PC were placed in an aluminum pan, sealed, and heated from 30 °C to 270 °C at a heating rate of 3 °C min^{-1}. Nitrogen was used as a purge gas at 50 mL min^{-1}. The data and DSC measurements were obtained using the TRIOS software platform. The first, second, and third peak temperatures (T_{peak}) between 30 and 100 °C, 100 and 200 °C, and 200 and 270 °C, were taken, respectively.

2.2.9. Thermogravimetry

Thermogravimetry (TG) was performed using a simultaneous analyzer (SDT Q600, TA Instruments), that had been calibrated with an N_2 flow rate of 50 mL min^{-1} and a heating rate of 15 °C min^{-1} from 30 °C to 650 °C. About 5 mg of the samples CHT, CHT–C-PC, CHT–STPP–C-PC, and spray-dried C-PC were analyzed in platinum crucibles (Machado et al., 2024). Thermal events typically associated with moisture and residues were measured between 30 and 120 °C and 650 °C on TG curves, respectively. The first derivative of TG (DTG) curves and TG measurements, such as mass loss and thermal stability temperature (T_{onset} DTG), were obtained using the TRIOS software platform. The first and second mass losses were determined between 30 and 100 °C and 100–200 °C on TG curves. –.

2.2.10. Small-angle and ultra small-angle X-ray scattering

The samples in aqueous dispersion were analyzed using small-Angle X-ray scattering (SAXS) and ultra-Small-angle X-ray scattering (USAXS) techniques at the Cateretê beamline of the Brazilian Synchrotron Light Laboratory (LNLS), part of the Brazilian Center for Research in Energy and Materials (CNPEM). Experiments were performed using aqueous suspensions (5.5 mg mL^{-1}) of CHT, C-PC, CHT–C-PC, and CHT–STPP–C-PC.

A beam with a point source geometry of 55 μm and energy of 8 keV, corresponding to a wavelength of 1.5498 Å, was used. Data was obtained using a Medipix3 detector (PITEC) with a resolution of 3000 × 3000 $pixels^2$. All measurements were taken using a Sirius' accelerator, which operates with two novel superconducting radio-frequency cavities capable of high-power frequency generation (240 kW, 200 mA). The 2D scattering intensities were azimuthally integrated providing a 1D curve of the intensity as a function of the momentum transfer modulus, *q*, defined as described in eq. 7.

$$q = 4\pi\, sen\frac{(\theta)}{\lambda} \quad (7)$$

where,2θ is the scattering angle and λ the radiation wavelength.

SAXS measurements were taken with a detector positioned 1.55 m from the sample, covering a scattering vector (q) range of 0.03 to 2.76

nm^{-1}. USAXS measurements were taken with the detector placed 15.0 m from the sample, enabling access to a q-range of 0.003 to 0.347 nm^{-1}. All the experiments were conducted at a controlled temperature of 25 °C. The final treated scattering curves were merged to a single profile.

2.2.11. Nitrogen adsorption isotherms

Nitrogen adsorption–desorption isotherms (NAI) data were obtained using a Micromeritics ASAP 2020 instrument. Before analysis, the samples were degassed (<10 μm Hg) at 40 °C. The nitrogen adsorption was analyzed at a temperature of −196 °C. The obtained isotherms were analyzed using the BET (Brunauer–Emmett–Teller) method to determine the specific surface area and the BJH (Barrett–Joyner–Halenda) method with the KJS (Krug–Jaroniec–Sayari) thickness equation to determine pore size distribution values (Rasmussen et al., 2021).

2.2.12. Characterization and stability of free C-PC

The colorimetric and fluorometric properties of C-PC, as well as its stability under varying pH and temperature conditions, were assessed in triplicate with blanks as follows. The absorbance spectra of C-PC was evaluated at a concentration of 0.2 $mg{\cdot}mL^{-1}$ at pH 6.0 (in potassium phosphate buffer, PB, 50 mM) at 25 °C from λ 310 to 760 nm using an EnSpire® Multimode Plate Reader (Perkin-Elmer®), with 200 μL per well in a 96-well microplate at 1 nm intervals and. A calibration curve was constructed using the same instrument (**Fig. S7**, **Supporting Information – SI**) by measuring absorbance at λ 620 nm (the maximum absorbance wavelength of C-PC) for samples at various concentrations.

Fluorescence analysis of C-PC (0.08 $mg{\cdot}mL^{-1}$ in PB 50 mM) was performed using three-dimensional (3D) fluorescence spectroscopy with an RF-6000 spectrofluorometer (Shimadzu), using parameters adapted from Galván et al. (2024). Excitation wavelengths (λ_{ex}) ranged from 220 to 600 nm with 2-nm increments, while emission wavelengths (λ_{em}) ranged from 370 to 650 nm with 1-nm increments. Measurements were conducted at 25 °C ± 2 °C using quartz cuvettes with four polished faces, a volume of 3.5 mL, and a 10-mm optical path. Excitation and emission spectra were extracted from the 3D fluorescence maps.

Colorimetric analysis (L*, a*, b* coordinates and turbidity) was performed using a CM-5 spectrophotometer (Konica Minolta) after calibrating the CIE-L*a*b color system against white and black backgrounds. Measurements were performed on 3–mL sample solutions in transparent plastic cells with a 2-mm path length (CM-A130). Color differences (ΔE) were calculated using the CIEDE2000 system via the ColorMine.org platform.

Stability was analyzed by assessing absorbance spectra of C-PC (0.2 $mg{\cdot}mL^{-1}$) under various pH, temperature, and time conditions. For temperature analyses, samples were prepared at pH 6.0 ± 0.1 and incubated at 25 °C, 50 °C, 60 °C, and 70 °C, before measurements were taken after 0.5 h, 1 h, 2 h, and 2.5 h. To evaluate the effect of pH, samples were prepared at pH values of 2, 4, 6, 8, 10, and 12 (±0.2), incubated at 25 °C for 30 min, before analysis. The pH was measured using a benchtop pH meter (QUIMIS), calibrated with commercial pH 4.00 and 7.00 buffers, and adjusted by dropwise addition of 0.1 M NaOH or HCl solutions while continuously monitoring the pH, prior to the dissolution of C-PC.

2.2.13. Effect of encapsulation on C-PC colorimetric and fluorometric properties

The effect of encapsulation on colorimetric and fluorometric properties and stability of C-PC was evaluated by the following procedure. Free C-PC, CHT–C-PC, and CHT–STPP–C-PC were resuspended in purified water and adjusted to an initial absorbance of 0.3 AU at λ 620 nm (0.2 $mg{\cdot}mL^{-1}$ of C-PC) for absorbance and colorimetric analyses, and to 0.1 AU at λ 620 nm (0.08 $mg{\cdot}mL^{-1}$ of C-PC) for fluorescence analysis.

The thermal stability of the formulations was assessed by incubating the samples at 25 °C and 70 °C for 30 min at pH 6.0 ± 0.1 in PB 50 mM pH 6.0. The effect of pH was investigated by adjusting aqueous solutions to pH 2.0 ± 0.1, 6.0 ± 0.1, and 10.0 ± 0.1, as previously stated in Section 2.2.12, before dissolving C-PC and incubating it at 25 °C for 30 min. Stability under storage was evaluated by incubating the samples at 25 °C and pH 6.0 ± 0.1 in PB 50 mM for 30 min, two weeks under light exposure (450 ± 10 Lux, measured with a digital lux meter BSIDE L1, with a range of 0.1 to 200,000 lx), and four weeks in darkness.

All the samples were subjected to absorbance spectra analysis, 3D-fluorescence spectroscopy (in triplicate), and colorimetry (ΔE CIE 2000, turbidity, and visual color representation) as described in Section 2.2.12.

Thermal stability kinetics of free C-PC and CHT–C-PC were evaluated under controlled conditions (±0.5 °C). Samples were adjusted to an initial absorbance of 0.3 AU at $\lambda_{620\ nm}$, and then subjected to thermal stress at 65, 75, 85, and 95 °C for 0, 0.25, 0.5, 1, 2, 4, 8, and 24 h. Additionally, kinetic analyses were performed assuming a second-order degradation model, according to eq. 8.

$$\frac{1}{[A]} = \frac{1}{[A]_0} + kt \tag{8}$$

where [A] is the absorbance at 620 nm at time t, $[A]_0$ is the initial absorbance, k is the second-order degradation rate constant, and t is the reaction time.

The second-order kinetic model was also applied to the three time points obtained from the long-term stability experiment performed at 25 °C.

The experimental half-life ($t_{1/2}$) was determined directly from the raw absorbance data. For each temperature, the initial absorbance (C_0) corresponded to the value measured at $t = 0$. The time at which the absorbance reached 50 % of C_0 ($0.5{\cdot}C_0$) was identified, and $t_{1/2}$ was calculated by linear interpolation between the two consecutive time points surrounding this value. This approach provides a model-independent estimate of $t_{1/2}$, reflecting the actual degradation profile of the samples.

2.2.14. Application of encapsulated C-PC on Gelatin dessert

Free C-PC, CHT–C-PC, and CHT–STPP–C-PC were separately dissolved in water to reach an absorbance of 0.6 AU at λ 620 nm, corresponding to 0.4 $mg{\cdot}mL^{-1}$ of C-PC. These solutions were mixed at a 1:1 ratio with either water (control) or a colorless and flavorless gelatin solution [type B gelatin (from bovine skin and bones) Dr. Oetker, 48 $mg{\cdot}mL^{-1}$, 40 °C], resulting in final concentrations of 0.2 $mg{\cdot}mL^{-1}$ for C-PC and 24 $mg{\cdot}mL^{-1}$ for gelatin. The gelatin had previously been dissolved in water and maintained at 40 °C for 20 min to ensure complete homogenization before incorporation of free or encapsulated C-PC. The control (water, 25 °C, day 0) was maintained at 25 °C for 30 min. The samples containing free or encapsulated C-PC in gelatin were heated at 100 °C for 15 min. Absorbance spectra were recorded from λ = 450 to 700 nm (1 nm increments, 200 μL per well) using an EnSpire multimode plate reader (Perkin-Elmer) at 0, 6, and 22 days of storage at 4 ± 2 °C. Before each measurement, samples were equilibrated at 25 °C for 30 min to allow temperature stabilization. Results were presented as the average of triplicate measurements, after blank subtraction (water or gelatin). The second-order kinetic model, described in section 2.2.13, was also applied to present the results.

2.2.15. Statistical analysis

All experiments were performed in triplicate, and data are expressed as mean ± standard deviation (SD). Statistical analyses were conducted to compare the physicochemical parameters between the two formulations (CHT–C-PC and CHT–STPP–C-PC). A two-tailed Student's *t*-test was applied to evaluate significant differences ($p < 0.05$). Statistical analyses were performed using GraphPad Prism version 10.0 (GraphPad Software, San Diego, CA, USA).

3. Results and discussion

3.1. C–PC Encapsulation

The CHT–C-PC and CHT–STPP–C-PC presented similar particle sizes with diameters of about 3.8 μm (Table 1, Fig. 1, and **Fig. S1 – SI**). In contrast, particle shapes were visibly different. CHT–C-PC appeared compact and spherical, but CHT–STPP–C-PC displayed crushed-like defects.

Values represent mean ± standard deviation (n = 3). Different lowercase letters within the same column indicate statistically significant differences between formulations ($p < 0.05$) according to the two-tailed Student's t-test. <LQ: less than the limit of detection. CHT–C-PC refers to chitosan–C-phycocyanin microparticles, while CHT–STPP–C-PC refers to those prepared with sodium tripolyphosphate (STPP).

Spray-drying low molecular weight chitosan (50–190 kDa) from diluted acids typically results in microparticles with internal diameters ranging from 1 to 10 μm (Alhalaweh et al., 2009; Desai & Park, 2005a; Milenkova et al., 2024). The small particle sizes obtained in this study (i.e., ~3.8 μm of internal diameter) can be useful in foods, cosmetics, and drugs for uniform dispersion, which prevents processing issues that might compromise texture and sensory properties (Meng et al., 2023). The presence of STPP in CHT–STPP–C-PC implies that electrostatic interactions between anionic tripolyphosphates and protonated amino groups of chitosan linear chains form a phosphorylated polyelectrolyte hydrogel. When atomized by compressed and heated air, the liquid CHT–STPP–C-PC preparation is disrupted, resulting in droplets that immediately lose their solvent system by evaporation. The phosphorylation reactions form typical crushed-like microparticles. These observations are aligned with the recorded phosphorous content in CHT–STPP–C-PC (Table 1) and findings of previous studies on the effect of crosslinking agents on spray-dried chitosan microparticles (Desai & Park, 2005b; Helbling et al., 2018).

The process yields for CHT–C-PC and CHT–STPP–C-PC were approximately 37 % (Table 1), which are in line with previously reported yields of spray-dried chitosan microparticles (Alhalaweh et al., 2009; Desai & Park, 2005a; Desai & Park, 2005b; Milenkova et al., 2024). Such modest yields are commonly observed in spray-drying of polysaccharide-based materials, including chitosan, mainly due to the loss of fine particles that remain entrained in the exhaust air or adhere to the chamber and cyclone walls. Aranaz et al. (2017) reported that these losses are primarily associated with particle adhesion to the cyclone surfaces and the escape of small, lightweight fractions through the exhaust system, while Katsarov et al. (2017) observed process yields ranging from 37 % to 64 %, depending on feed viscosity and atomization rate. These findings indicate that the relatively low yield obtained in this study (~37 %) likely results from the combined effects of low feed viscosity, fine droplet formation, and partial particle loss during drying.

In contrast to the process yields, the %EE were notably different, as CHT–STPP–C-PC retained almost twice as much C-PC and CHT–C-PC (Table 1). STPP crosslinking of chitosan linear chains has been associated with increasing %EE because it increases the viscosity of the solution (Desai & Park, 2005a) and promotes physical entrapment for C-PC molecules. In our system, this improvement is attributed to the formation of a denser and more cohesive polymeric network. During drying, electrostatic interactions occur between the anionic tripolyphosphate groups and the protonated amino groups of chitosan, leading to ionic crosslinking. This structural arrangement reduces the free volume inside the droplets and limits the diffusion of C-PC, thereby improving its retention within the microparticles. Comparable increases in %EE have been reported for chitosan-based systems containing food-grade proteases (~78.6 %, Busto et al., 2022) and bovine serum albumin (50–87 %, Kusonwiriyawong et al., 2013), both obtained by spray drying under low-viscosity conditions. The formation of denser ionic or polyelectrolyte networks has been shown to limit molecular mobility (Kašpar et al., 2013) and enhance protein retention within the chitosan matrix.

The ζ of CHT–C-PC was 20 mV higher than that of CHT–STPP–C-PC (Table 1). Therefore, the CHT–C-PC may have higher colloidal stability than CHT–STPP–C-PC as ζ values higher than ±30 mV are typically associated with stable systems (Lemos et al., 2020). These findings are crucial for further applications of the C-PC microparticles as colorants in foods and cosmetics to prevent issues related to coloring changes caused by their aggregation over time. Apart from indicating colloidal stability, ζ also indicates the extent of phosphorylation reactions such as crosslinking on the surfaces of microparticles (Wongsagonsup et al., 2005). The expressive decrease of ζ (Table 1) can be attributed to the presence of STPP in CHT–STPP–C-PC corroborating findings of previous studies on SEM, %EE, and %P.

C-PC encapsulation within chitosan-based microparticles was achieved with a notable effect of tripolyphosphate anions on the shapes of microparticles and %EE.

Table 1
Yield, encapsulation efficiency (% EE), particle average internal diameter, zeta potential (ζ), and phosphorous content (%P) of the microparticles.

Microparticles	Yield (%)	%EE	Diameter (μm)	ζ (mV)	%P
CHT–C-PC	37.77 ± 1.11[a]	36.71 ± 0.49[a]	3.87 ± 1.25[a]	44.53 ± 1.25[a]	<LQ[a]
CHT–STPP–C-PC	35.26 ± 1.10[a]	72.91 ± 4.91[b]	3.64 ± 1.03[a]	24.5 ± 2.45[b]	1.38 ± 0.05[b]

3.2. Fourier-transform infrared spectroscopy coupled with attenuated Total reflectance

FTIR–ATR was used to examine chemical interactions in chitosan-based microparticles, assuming representative sampling across particle surfaces and near-core regions (penetration depth ~ 0.5–2.0 μm, Harrick, 1967, Sevenou et al., 2002, Gieroba et al., 2022, Paluszkiewicz et al., 2011). The spectra and absorption indices of CHT, CHT–C-PC, CHT–STPP–C-PC, and spray-dried C-PC are presented in Fig. 1 and Table 2. CHT showed the following characteristic bands: broad N–H/O–H stretch (3600–3000 cm^{-1}), C—H stretch (2921, 2877 cm^{-1}), amide I/II (1645, ~1550 cm^{-1}), CH_2/CH_3 bending (1423, 1375 cm^{-1}), and intense polysaccharide backbone signals (1300–1000 cm^{-1}) (Galván et al., 2024; Machado et al., 2024; Queiroz et al., 2014). Spray-dried C-PC spectra matched those reported in previous studies (Lemos et al., 2020).

CHT–C-PC and CHT–STPP–C-PC spectra exhibited notable shifts and band intensity changes when C-PC incorporated. Surface-level IR regions (3600–2800 cm^{-1}) revealed overlapping C-PC and CHT bands with evolved A2932/A2874 ratios (**Fig. S2A – SI**, Table 2). In the intermediate region (1800–1300 cm^{-1}), variations in the A1651/A1545 index indicated altered amide I/II contributions, suggesting changes in protein conformation and interaction with chitosan (**Fig. S2B – SI**, IMB Jena Image Library, 2025). Additional shifts (e.g., 1423 → 1407 cm^{-1}, 1375 → 1382 cm^{-1}) were absent in C-PC alone, reinforcing composite formation. **Fig. S2 (C) – SI**). Deeper core signals (1300–1000 cm^{-1}) showed minimal differences due to overlapping chitosan bands and lack of phosphorus signal resolution.

Overall, FTIR confirmed chemical interactions between chitosan and partially negative C-PC (pI 4.6–5.2 in acidic pH) to form supramolecular structures. These interactions complemented physical entrapment and were enhanced by STPP crosslinking (see section 3.2). The spectral changes across particle layers suggest uniform C-PC dispersion and structural integration, consistent with SEM findings.

3.3. X-ray diffractometry

XRD patterns of spray-dried and control samples are shown in Fig. 1. Chitosan typically exhibits peaks at 10.0° and 20.0° 2θ, corresponding to

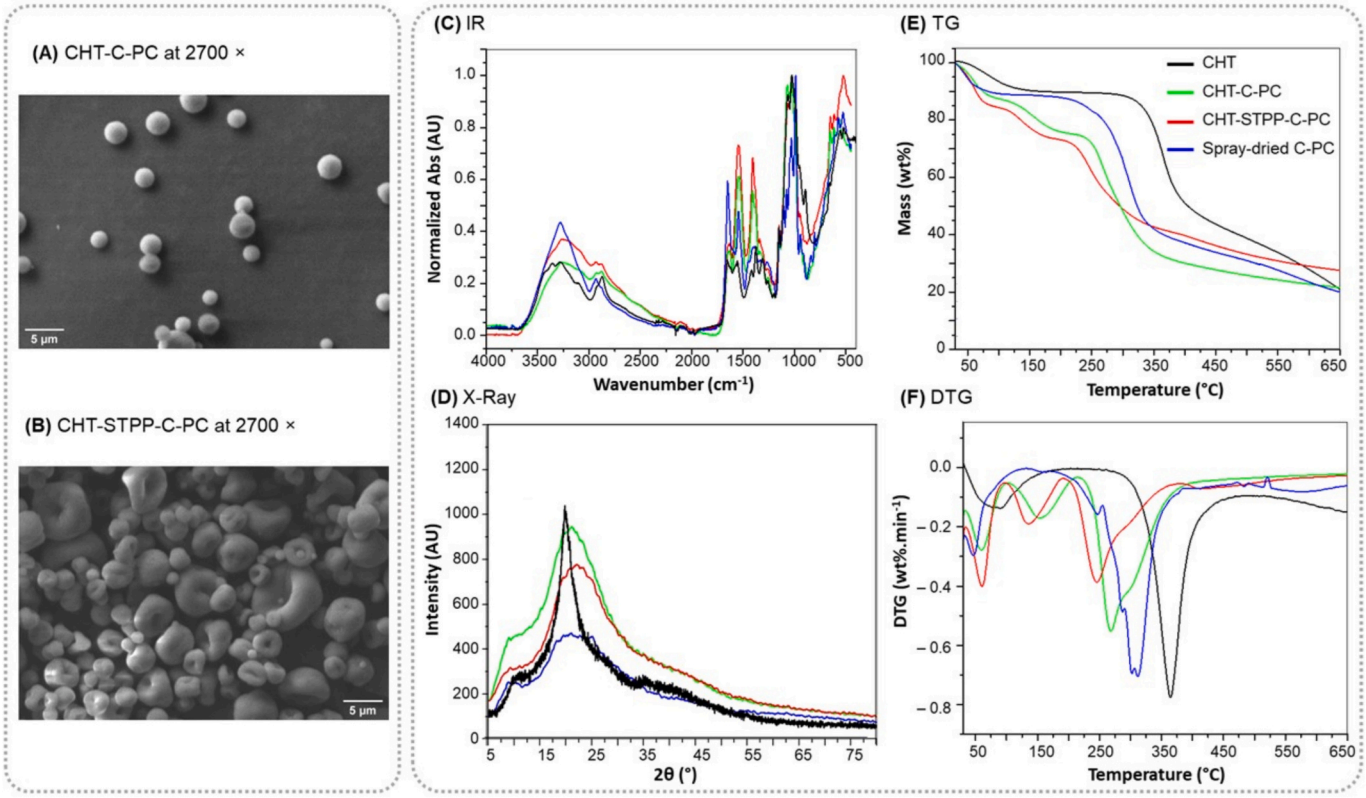

Fig. 1. Micrographs of (A) CHT–C-PC and (B) CHT–STPP–C-PC microparticles at a magnification of 2700×. (C) Infrared spectra, XRD, TG, and DTG curves of CHT–C-PC, CHT–STPP–C-PC, spray-dried C-PC, and CHT samples. CHT refers to chitosan microparticles, while spray-dried C-PC denotes C-phycocyanin after spray drying. CHT–C-PC refers to chitosan–C-phycocyanin microparticles, and CHT–STPP–C-PC refers to chitosan–sodium tripolyphosphate–C-phycocyanin microparticles (STPP).

Table 2
Infrared absorption indices and thermal properties of CHT–C-PC, CHT–STPP–C-PC, spray-dried C-PC, and CHT. First and second mass loss events occurred between 30 °C and 100 °C, and 100 °C and 200 °C, T_{onset} DTG, and residues. First, second, and third peak temperatures were taken between 30 °C and 100 °C, 100 °C and 200 °C, and 200 °C and 270 °C, respectively.

Sample	FTIR-ATR			TG				DSC		
	A_{2932}/A_{2874}	A_{1651}/A_{1545}	A_{1407}/A_{1382}	First mass loss (%)	Second mass loss (%)	T_{onset} DTG (°C)	Residue (%)	First T_{peak} (°C)	Second T_{peak} (°C)	Third T_{peak} (200–270 °C)
CHT–C-PC	1.03	0.51	1.12	14.8	11.2	231.9	21.6	56.0	153.0	253.1
CHT–STPP–C-PC	0.98	0.46	1.20	17.1	11.0	215.7	27.5	59.0	140.8	237.1
Spray-dried C-PC	1.19	1.24	1.00	12.8	–	207.9	19.9	56.5	–	235.8
CHT	0.80	1.10	0.73	9.67	–	301.5	20.8	60.4	–	–

sym. Symmetric; *asym*. Asymmetric. C—H sym./ C—H a*sym* (A_{2932}/A_{2874}). Amide *I*/ Amide II (A_{1651}/A_{1545}). CH_2 bending/ CH_3 sym.

the (002) and (101) planes (Antonino et al., 2017), as observed in the control (black line). These peaks arise from intra- and inter-molecular hydrogen bonding in the crystalline domains of chitosan. Dissolution in acetic acid disrupts these interactions, and subsequent spray-drying alters crystallinity depending on solvent evaporation rates (Cervera et al., 2011).

Spray-drying had a remarkable impact on chitosan and C-PC crystalline structures. We observed a peak broadening at 20.0 2θ ° of CHT–C-PC and CHT–STPP–C-PC relative to CHT starting material, in contrast to the peak at 10.0 2θ °. Additionally, structure amorphization seemed more evident in CHT–STPP–C-PC, with no obvious diffractions from free STPP salt. These findings are consistent with structural amorphization caused by a fast solvent system withdrawal typical of a spray-drying process, resulting in a residual chitosan crystallinity and C-PC amorphization on CHT–C-PC and CHT–STPP–C-PC samples.

The broad peaks at 10° and 20° suggest formation of a hydrated chitosan polymorph (Prashanth et al., 2002), and partial crystallinity owing to the moderate inlet temperature of 110 °C. Our findings are in line with the typical requirement of >120 °C for complete amorphization. In summary, spray-drying yielded a semi-crystalline CHT–C-PC hydrogel. XRD results aligned with FTIR, reflecting structural rearrangements driven by hydrogel formation.

3.4. Thermal analysis

TG and DTG curves of the spray-dried and control samples are displayed in Figs. 1 **(E)** and **(F)**. Two main thermal events were observed in both chitosan and spray-dried C-PC, the first corresponding to water evaporation and the second to thermal decomposition. Although both chitosan and spray-dried C-PC exhibited similar moisture content (~11

%), chitosan showed significantly higher thermal stability, with T_{onset} DTG values nearly 100 °C above those of C-PC (Table 2). This difference is consistent with chitosan's higher molecular weight and crystallinity (Patel et al., 2005).

Water sorption behavior differed between materials. There was a broad DTG peak near 100 °C for chitosan, suggesting the presence of crystallized and weakly bound water. In contrast, spray-dried C-PC showed a sharp DTG peak, and a distinct endothermic event in its DSC curve (**Fig. S3 – SI**), typical of amorphous materials. Chitosan degradation typically begins around 300 °C due to the decomposition of glucosamine and acetylglucosamine units, followed by breakdown of the glycosidic backbone (Machado et al., 2024). In contrast, C-PC begins decomposing near 250 °C (Lemos et al., 2020), with its T_{onset} DTG reduced to 207.9 °C after spray drying. This thermal degradation pattern was further supported by the absence of exothermic transitions in chitosan's DSC curve up to 270 °C (**Fig. S3 – SI**), whereas clear decomposition peaks were observed in C-PC.

The CHT–C-PC and CHT–STPP–C-PC microparticles exhibited more distinct thermal behavior, characterized by three thermal events, than the control samples. The first event, occurring between 30 °C and 100 °C, corresponded to water evaporation and accounted for about 16 % of the mass loss. The second event, between 100 °C and 200 °C, involved about 11 % mass loss, attributed to the release of retained acetic acid. This interpretation is supported by DTG peaks observed near 60 °C and 150 °C (Fig. 1F), as well as broad endothermic signals in the DSC curves at similar temperatures (**Fig. S3 – SI**). This behavior is consistent with solvent retention due to chitosan's affinity for water and acetic acid, and with the spray-drying inlet temperature of 110 °C.

The third and main thermal event occurred above 200 °C and was associated with about 43 % mass loss, reflecting the thermal decomposition both of chitosan polysaccharides and C-PC protein chains. DTG curves confirmed this decomposition onset, and DSC curves showed exothermic peaks around 244 °C (**Fig. S3 – SI**, Table 2). Although the microparticles were more thermally stable than spray-dried C-PC, their resistance remained lower than that of pure chitosan, indicating a modified structural organization resulting from C-PC incorporation. Although no specific thermal transitions attributable to phosphorus were observed, the higher residual mass in CHT–STPP–C-PC (~27 %) most likely reflects the presence of residual polyphosphates following pyrolysis.

Overall, thermal analysis revealed that the raw materials and the microencapsulated systems had distinct decomposition profiles. The additional intermediate thermal events observed in CHT–C-PC and CHT–STPP–C-PC reflect the integration of solvents and the formation of supramolecular structures. These findings support the structural modifications inferred from FTIR and XRD data, confirming the protective role of the chitosan matrix in stabilizing thermosensitive compounds such as C-PC.

3.5. *Small angle and ultra-small angle X-ray scattering*

The merged SAXS/USAXS profiles of spray-dried and control samples are shown in Fig. 2.

The intensities of the curves indicate a final region in Fig. 2 that resembles a form factor contribution and exhibits a steep increase in scattering intensity. This is a sign of a possible decoupling between the average form factor of the system and the structure factor. For this reason, we modeled the particles form factor and the system structure factor using the generalized indirect Fourier transformation (WGIFT, Oliveira, 2016, Oliveira et al., 2009) and a model for aggregated spheres.

The WGIFT modeling approach (Oliveira et al., 2009) allows the description of the form factor P(q) of internal structures and the structure factor S(q) of supramolecular aggregates. The form factors are described using the pair distance distribution function, p(r), which provides important indications about the particle shape (Glatter, 1977;

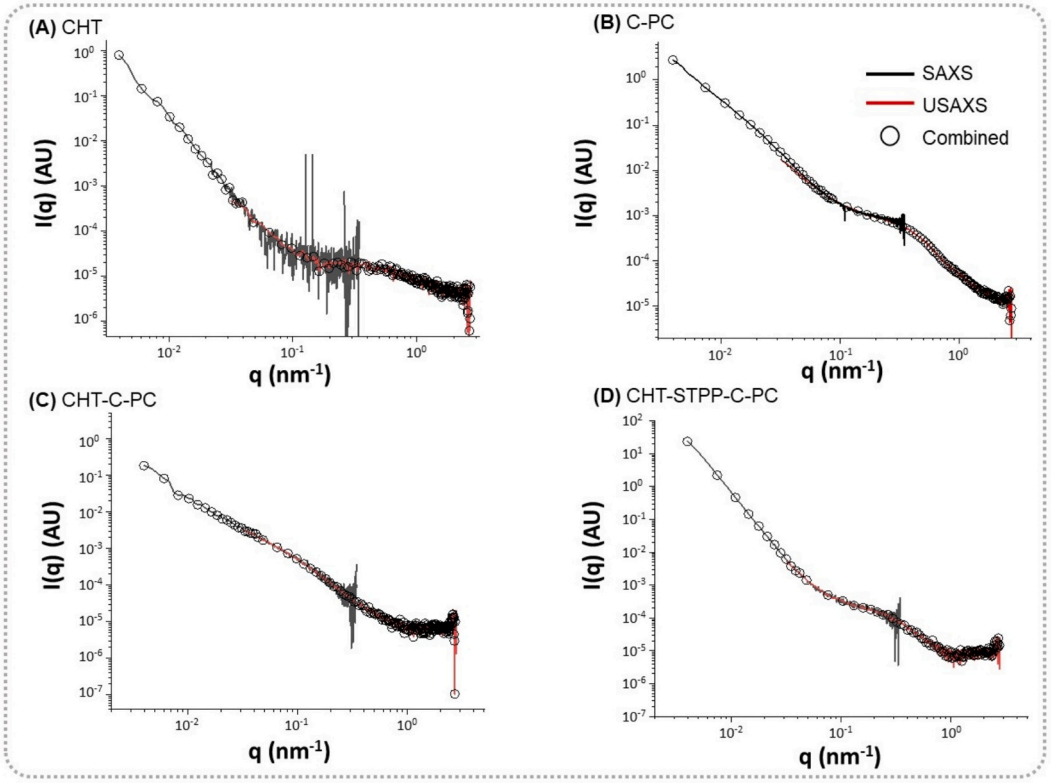

Fig. 2. Merged USAXS/SAXS data for CHT–C-PC, CHT–STPP–C-PC, C-PC, and CHT. CHT refers to chitosan microparticles, while C-PC denotes C-phycocyanin. CHT–C-PC refers to chitosan–C-phycocyanin microparticles, while CHT–STPP–C-PC refers to those prepared with sodium tripolyphosphate (STPP).

Oliveira, 2011) as shown in eq. 9.

$$P(q) = 4\pi \int_0^{D_{max}} p(r) \frac{\sin(qr)}{qr}\, dr \quad (9)$$

The final intensity is given by eq. 10, following the decoupling approximation described by Kotlarchyk & Chen, 1983.

$$I(q) = S_c\, P(q)\left(1 + \beta(q)\left[S_{frac}(q) - 1\right]\right) \quad (10)$$

where the decoupling approximation was used. Sc is an overall scale factor and β(q) is a factor that may describe the particle anisotropy and polydispersity. After several tests, the best structure factor that described the experimental data was a fractal structure factor (Oliveira, Monteiro, & Neto, 2014, Teixeira, 1988) as shown in eq. 11.

$$S_{frac}(q) = 1 + \frac{1}{(qR_0)^D} \frac{D\Gamma(D-1)}{\left[1 + \frac{1}{q^2\xi^2}\right]^{(D-1)/2}} \sin\left[(D-1)\tan^{-1}(q\xi)\right] \quad (11)$$

where $D(r, R, \sigma)$ is the number distribution of sizes given by a Shulz-Zimm Distribution (Pedersen, 1997).

The SI show the WGIFT modeling results and corresponding pair distribution functions are shown in **Figs. S4** and **S5**. These provide a good fit to the experimental data. Modeling using the aggregated spheres approach also yielded satisfactory fits (**Figs. S6** and **S7**). Despite the system's polydispersity, the pair-distance distribution function p(r) remained informative (Loh & Elser, 2009), indicating average particle dimensions and internal morphology (Pinto, 2011).

For the pure CHT microparticles, the analysis revealed small particles about 60–80 Å in diameter and large clusters with a fractal dimension of 2.9, a maximum size of 2900 Å, and internal substructures about 90 Å in size (Table 3). For C-PC, the data indicated larger particles (~180 Å) and the formation of extensive fractal aggregates with a fractal dimension of 2.6, an overall size of 1500 Å, and subunits with a radius of about 125 Å. The CHT–STPP–C-PC system exhibited a fractal dimension of 3.0, with aggregates reaching up to 5000 Å and subunits with a radius of about 80 Å. In contrast, CHT–C-PC showed a fractal dimension of 2.27, with smaller aggregate sizes (~600 Å) and subunits of about 113 Å. For CHT–C-PC, the initial region of the scattering curve was not well captured by the model, indicating limitations in fitting low-q data.

The aggregated polydisperse spheres model corroborated the WGIFT findings, yielding consistent values for fractal dimensions and aggregate sizes. However, accurate determination of the fractal subunit radius was hindered by the concurrent fitting of the form factor of the particles present in the system.

Small- and ultra-small-angle X-ray scattering (SAXS/USAXS) analyses revealed the internal architecture of the chitosan-based microparticles. The control sample of microparticles (CHT) exhibited a heterogeneous internal morphology characterized by interconnected channels or pores consistent with the proposed structural models. These features displayed characteristic correlation lengths (ζ) and fractal dimensions (D) consistent with volume-percolated domains. These findings are consistent with a volume fractal regime, suggesting the presence of multiscale porous networks spanning the microparticle interior. Such internal channels seem to act as reservoirs for C-PC, in agreement with previous findings of loading efficiencies of porous chitosan matrices exceeding 90 % (Sergeeva et al., 2023b). These findings confirm the role of pores in protein retention and potential controlled-release applications. A schematic illustration of the structural model is shown in Fig. 3.

The SAXS/USAXS data also provides important practical insight into how the internal organization of the chitosan matrix influences C-PC stabilization. The high fractal dimension observed for CHT–STPP–C-PC (D ≈ 3.0) indicates a more compact and interconnected network, which is consistent with a denser ionic crosslinked structure formed by TPP bridging between chitosan chains. Such an arrangement likely reduces the free volume and limits molecular diffusion, thereby improving the physical entrapment and retention of C-PC within the microparticles. In contrast, the lower D value for CHT–C-PC (D ≈ 2.3) suggests a looser and less percolated structure, which may allow greater water penetration and faster pigment release under stress conditions. These results are in agreement with previous SAXS-based studies showing that higher fractal dimensions (D ≈ 3) correspond to more space-filling and interconnected networks, characteristic of dense biopolymer assemblies (Mezzenga & Fischer, 2013).

C-PC also formed aggregates, which were generally smaller than those observed in the CHT microparticles (Table 3). These findings suggest that both C-PC molecules and their aggregates can penetrate and occupy the internal channels of the CHT–based microparticles.

For CHT–C-PC, both modeling approaches indicated the presence of a two-dimensional fractal structure (D ~ 2.0) and a smaller fractal domain size than that CHT–STPP–C-PC. These results support the hypothesis that STPP (present only in CHT–STPP–C-PC) interacts with chitosan chains, influencing the final structure of the system at both nano- and microscale levels. In CHT–STPP–C-PC, there was also a volume fractal (D ~ 3.0) and a larger fractal domain size, suggesting that protein incorporation enhanced both percolation and the extent of fractal domains. These structural observations are consistent with the morphological differences between CHT–C-PC and CHT–STPP–C-PC (Fig. 1), the presence of phosphorus exclusively in CHT–STPP–C-PC (Table 1), the encapsulation efficiency (%EE), which was twice higher in CHT–STPP–C-PC than in CHT–C-PC, and the ζ value, which was approximately half in CHT–STPP–C-PC relative to CHT–C-PC (Table 1).

These findings were further supported by NAI, which provided complementary evidence of the porous architecture inferred from SAXS/USAXS. Despite the overall low BET surface areas (0.0166–1.367 m^2/g) and pore volumes (0.000173–0.003483 cm^3/g) observed for all samples, the NAI profiles were consistent with a hierarchical porous structure dominated by macropores (Rouquerol et al., 2014). This is in agreement with the volume fractal regime (D ~ 3.0) and extensive percolation networks revealed by the scattering data. The minimal presence of micro- and mesopores, as indicated by the limited BJH peaks (3–15 nm), supports the notion that most voids are larger than 50 nm and, therefore, not accessible to nitrogen gas (Thommes et al., 2015). Such structures are typical of aggregated systems where voids arise from interparticle spacing rather than intrinsic material porosity (Svergun & Koch, 2003).

Notably, CHT–STPP–C-PC exhibited slightly higher pore volume in NAI measurements, which correlates with its larger fractal domain size and improved internal homogeneity. These results indicate the role of

Table 3
Model parameters obtained from generalized indirect Fourier transformation model and aggregated spheres model.

Sample	WGIFT			Aggregated spheres model				
	D	ζ (Å)	R_0 (Å)	D	ξ (Å)	R_0 (Å)	R (Å)	σ (Å)
CHT–C-PC	2.27 ± 0.01	600 ± 50	113 ± 2	1.83 ± 0.52	1600 ± 500	25 ± 10	31 ± 15	15 ± 3
CHT–STPP–C-PC	3.00 ± 0.01	5000 ± 1000	80 ± 10	3.00 ± 0.01	3000 ± 500	20 ± 10	30 ± 15	15 ± 2
C-PC	2.59 ± 0.01	1500 ± 30	125 ± 1	2.50 ± 0.01	1900 ± 100	30 ± 10	17 ± 3	11 ± 1
CHT	2.91 ± 0.01	2900 ± 300	94 ± 2	2.98 ± 0.01	2500 ± 500	20 ± 10	15 ± 10	5 ± 2

Values represent mean ± standard deviation ($n = 3$). CHT refers to chitosan microparticles, while C-PC denotes C-phycocyanin. CHT–C-PC refers to chitosan–C-phycocyanin microparticles, while CHT–STPP–C-PC refers to those prepared with sodium tripolyphosphate (STPP).

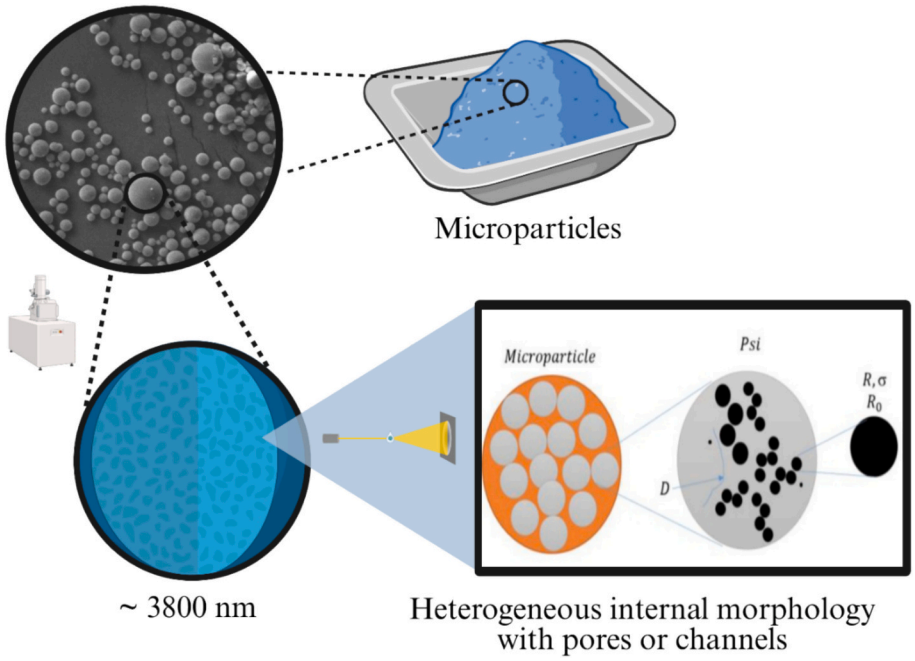

Fig. 3. Schematic representation of the microparticles described by the WGIFT and aggregated spheres models.

STPP in enhancing crosslinking and stabilizing the porous network (Giroux et al., 2015). In contrast, the low-dimensional fractal structure and poor low-q fitting in CHT–C-PC are consistent with its negligible NAI porosity, suggesting the presence of collapsed or poorly interconnected pores.

Overall, the combined SAXS/USAXS and NAI analyses reveal, for the first time, the multiscale porous network structure of spray-dried chitosan–phycocyanin microparticles, whose architecture is strongly governed by formulation parameters, particularly TPP, with direct implications for their capacity to encapsulate and retain biomolecules such as C-PC.

3.6. Characterization of C-PC

The optical and physicochemical characteristics of free C-PC were determined to establish baseline properties and define critical stress conditions for evaluating encapsulated systems. The absorbance spectrum of C-PC (0.2 mg·mL^{-1}, pH 6.0, 25 °C) exhibited a major peak at

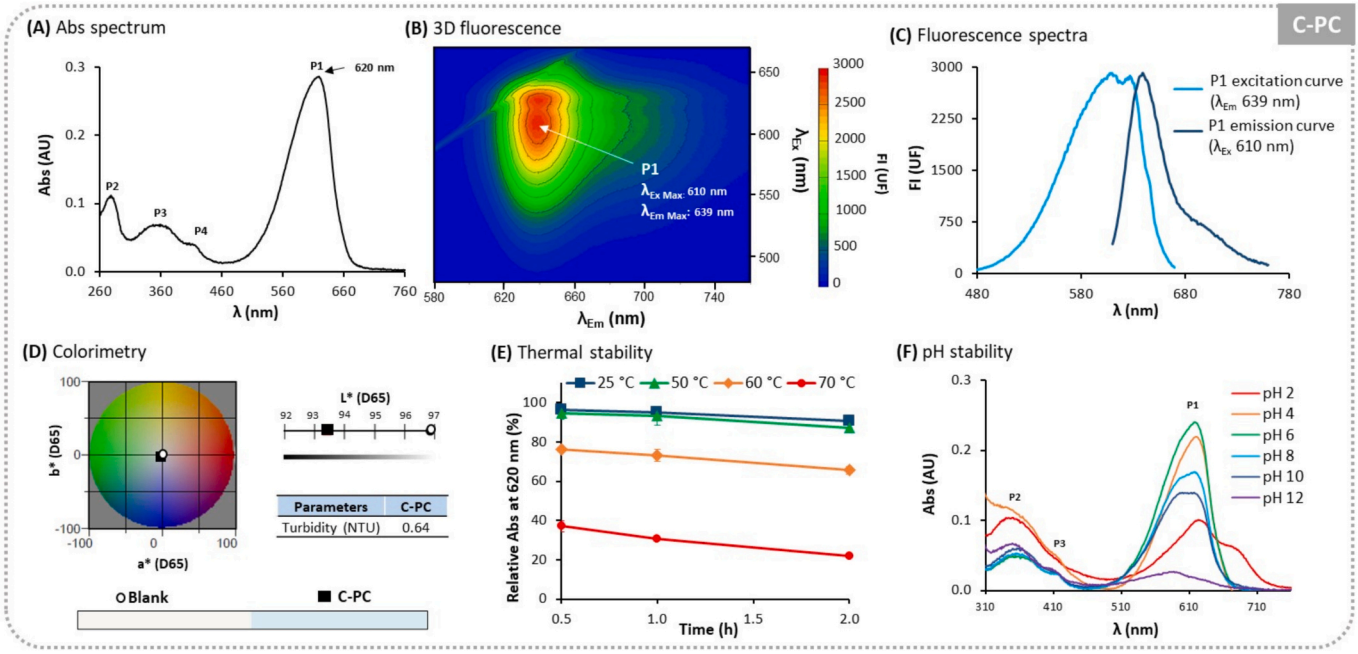

Fig. 4. C-PC characterization and stability. (A) Absorbance (Abs) spectrum of C-PC (0.2 mg· mL^{-1}). (B) 3D fluorescence spectra and (C) excitation (λEm 639 nm) and emission (λEx 610 nm) curves of C-PC (0.08 mg· mL^{-1}). (D) Color wheel, L* scale, turbidity, and color representation of the samples (Observer: 10°, Illuminant: D65) of C-PC (0.2 mg· mL^{-1}). (E) Relative Abs (at λ 620 nm) of C-CP (0.2 mg· mL^{-1}) at various times and temperatures (C-PC at 0,5 h and 25 °C as the reference). (F) Abs spectra of C-PC (0.2 mg· mL^{-1}) after 30 min at various pH values (±0.2). Except for (E), the temperature was maintained at 25 ± 2 °C, and except for (F), the pH of solutions was 6.0 ± 0.1.

620 nm (Fig. 4A), corresponding to its characteristic chromophore, and consistent with the findings of Lemos et al. (2020). A secondary band observed in the 260–300 nm range can be attributed to aromatic amino acids, such as tryptophan, phenylalanine, and tyrosine (Bai et al., 2023; Frank et al., 1978), known for their intrinsic absorbance and fluorescence properties (Santos et al., 2019). A minor peak near 360 nm was also observed and has been previously associated with partially dissociated or cyclic forms of the phycocyanobilin chromophore (AnaSpec, 2025, Böcker et al., 2020, Lauceri et al., 2019, Parshina et al., 2024).

Fluorescence analysis revealed a single excitation/emission pair with maxima at λ_{ex} 610 nm and λ_{em} 639 nm (Fig. 4B), consistent with previous reports for C-PC (Lemos et al., 2020). This spectral profile was further confirmed by excitation and emission curves derived from the 3D fluorescence map (Fig. 4C).

Colorimetric parameters in the CIE-Lab* system were L* = 93.01, a* = −5.16, and b* = −5.75 (Fig. 4D), indicating a slightly bluish tone. These values indicate lightness and chromaticity, where negative a* and b* confirm the blue-green nature of C-PC (Veríssimo et al., 2022). The turbidity of 0.64 NTU confirmed the clarity of the solution, an important attribute for food and cosmetic applications (Pathare et al., 2013).

Thermal stability was evaluated by incubating C-PC at 25, 50, 60, and 70 °C for up to 2 h. The colorant retained over 90 % of its absorbance at λ 620 nm at 25 °C and 50 °C, but a marked decline occurred at 70 °C, at which only 37.2 % of the initial signal remained after 30 min (Fig. 4E). Complete spectral profiles under each condition are shown in **Figs. S8–SI**. These results, which indicate thermal significant sensitivity, are consistent with previously reported melting temperatures of 57.5 °C (pH 7) and 61.8 °C (pH 5) for purified C-PC (Martelli et al., 2014). The absorbance drop is attributed to chromoprotein denaturation, which compromises the vivid blue color of purified C-PC (Wang et al., 2025). Based on these findings, 70 °C was selected as a reference condition for thermal stress in encapsulated systems.

The effect of pH was investigated at values 2, 4, 6, 8, 10, and 12 after 30-min incubation at 25 °C. Strong alterations in the spectrum (peak broadening, intensity loss, and shifts in λ_{max}) were observed under acidic (pH 2) and alkaline (pH 12) conditions (Fig. 4 **F**). These patterns are consistent with previously reported optimal C-PC stability between pH 5.5 and 6.0 (Adjali et al., 2022). Acidic conditions might lead to chromophore conformational rearrangements or protein precipitation, while alkaline pH can destabilize electrostatic and hydrophobic interactions within the complex (Nowruzi et al., 2022, Wang et al., 2025). Based on these results, pH values of 2 and 10 were used for subsequent stress testing of encapsulated formulations.

Results of control experiments confirmed that chitosan, the encapsulating matrix, did not interfere with spectroscopic or colorimetric analysis. Chitosan showed no detectable fluorescence at 1.5 mg·mL^{-1} and appeared white at 4.5 mg·mL^{-1}, confirming its optical neutrality (**Fig. S9 – SI**). Further discussion of spectral nuances and chromophore rearrangement is provided in **Section 3.6 – SI**.

3.7. Effect of encapsulation on C-PC colorimetric and fluorometric properties

The protective effect of chitosan-based encapsulation on C-PC was examined under thermal, pH, and storage stress (Fig. 5) conditions relevant to food, cosmetic, and pharmaceutical applications (Yuan et al., 2022). Samples of free C-PC, CHT–C-PC, and CHT–STPP–C-PC were analyzed using absorbance spectra, 3D fluorescence, and CIEDE2000-based color metrics. Expanded datasets and spectra are shown in **Figs. S10–S19 – SI**.

Spray-drying alone did not compromise C-PC stability (**Fig. S14 – SI**). Under heat (70 °C for 30 min), free C-PC retained <40 % of its absorbance at λ 620 nm, whereas encapsulated samples retained >70 % of their absorbance, indicating thermal protection by the matrices (Özkan & Bilek, 2014). Free C-PC showed poor thermal stability in the kinetic analysis (Fig. S20A–B), with rapid degradation at all tested temperatures. In contrast, CHT-C-PC (Fig. S20C–D) displayed markedly improved preservation of colorimetric properties, retaining >60 % of

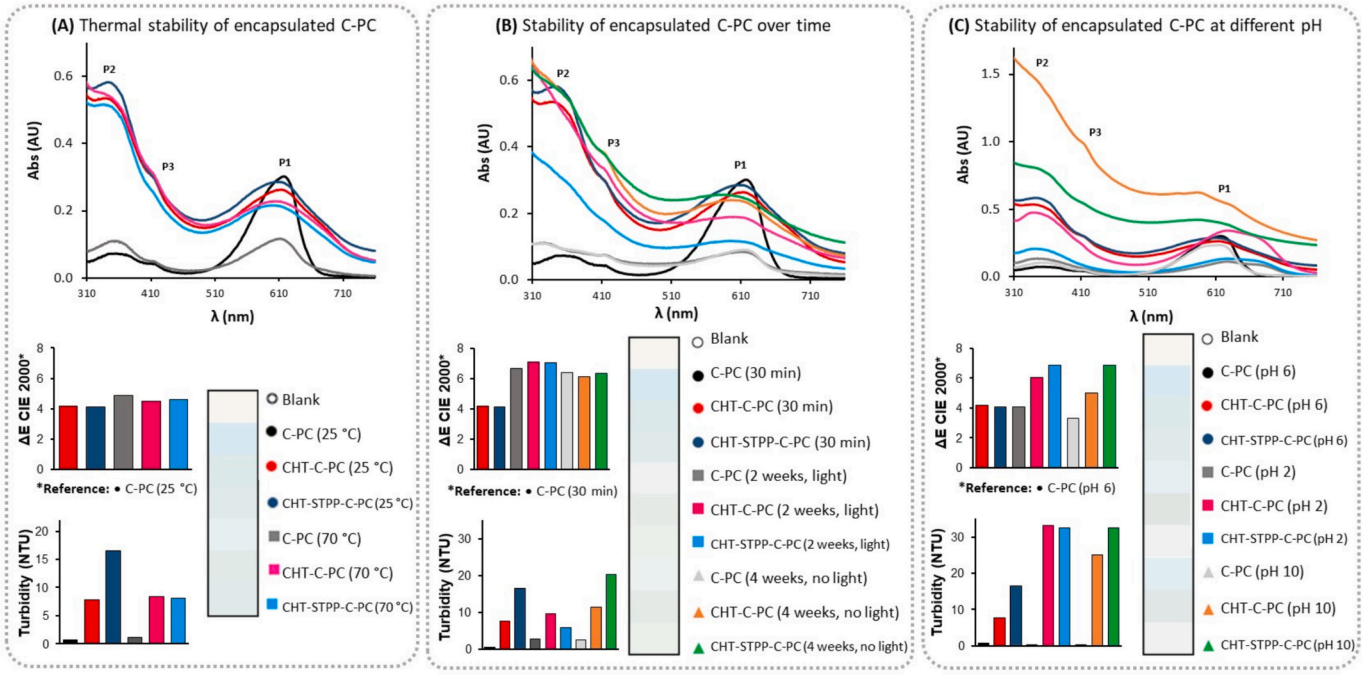

Fig. 5. Stability of encapsulated C-PC at various temperatures, times, and pH values. Absorbance (Abs) spectrum, ΔE CIE 2000, turbidity, and color representation of free-CPC, chitosan-C-phycocyanin (CHT–C-PC), chitosan-STPP-C–phycocyanin (CHT–STPP–C-PC)-based microparticles: (A) after 30 min at 25 °C or 70 °C in PB 50 mM pH 6.0; (B) after 30 min and 2 weeks at 25 °C with light exposure (450 ± 10 Lux), and 4 weeks without light at 25 °C in PB 50 mM pH 6.0, and (C) after 30 min in aqueous solutions at pH 6, pH 2, and pH 10 at 25 °C. Initial Abs of the samples was 0.3 AU at λ 620 nm (0.2 mg· mL^{-1} of C-PC). CHT refers to chitosan microparticles, while C-PC denotes C-phycocyanin. CHT–C-PC refers to chitosan–C-phycocyanin microparticles, while CHT–STPP–C-PC refers to those prepared with sodium tripolyphosphate (STPP).

the initial absorbance after 24 h at 65 °C and around 50 % after 4 h at 95 °C. Notably, CHT–C-PC maintained ~30 % of the initial absorbance even after 24 h at 95 °C, compared with <2 % for free C-PC. These trends are consistent with the experimental half-life values (Table S1), which show a sharp decrease in $t_{1/2}$ for free C-PC with increasing temperature, while encapsulation significantly prolongs thermal stability across all conditions. The second-order plots further confirm that the degradation rate of C-PC increases with temperature, and that encapsulation substantially slows the reaction.

As for the colorimetry analysis, a slight blue shift was observed in encapsulated forms even at 25 °C, suggesting matrix–chromophore interactions. However, the overall characteristic blue hue of C-PC was preserved after encapsulation, although the formulation became more turbid. Colorimetric differences (ΔE ~4 at baseline) increased after heating, but encapsulated samples maintained low ΔE and no increase in turbidity, with CHT–STPP–C-PC showing enhanced colloidal stability. Hence, this reflects a trade-off between increased turbidity and enhanced stability: while the higher light scattering may limit the use of CHT–C-PC in transparent systems such as clear beverages or visually clear gels, it simultaneously provides greater protection against thermal and photodegradation. As a result, the encapsulated colorant becomes especially suitable for opaque or semi-opaque applications, including thermally processed foods (e.g., jellies, puddings, baked products) and cosmetic emulsions where transparency is not required.

During storage, free C-PC underwent significant degradation, with ΔE >6 and turbidity increasing after two weeks of light exposure or four weeks in the dark. Encapsulated formulations showed higher retention of absorbance and color. CHT–C-PC preserved optical properties, while CHT–STPP–C-PC minimized turbidity, most likely due to network densification from STPP crosslinking.

Under pH stress (pH 2 and 10), free C-PC exhibited spectral disruption, whereas CHT–C-PC preserved absorbance more effectively, particularly at pH 2. CHT–STPP–C-PC was less effective under acidic conditions. The chitosan matrix most likely buffered local pH and stabilized the chromophore–protein complex (Andreeva et al., 2017; Galván et al., 2024). Full discussion and spectral data are provided in **Section 3.7 – SI**.

All encapsulated samples showed >90 % fluorescence quenching under stress most probably owing to restricted chromophore mobility and static quenching within the matrix (Tansi et al., 2015). Despite loss of fluorescence, absorbance at λ 620 nm remained intact, confirming structural preservation (Lemos et al., 2020; Martelli et al., 2014). While loss of fluorescence limits use in fluorescence sensing, encapsulation effectively stabilizes C-PC as a natural colorant.

3.8. *Application of encapsulated C-PC in gelatin dessert*

To assess their application as natural colorants, free and encapsulated C-PC (CHT–C-PC and CHT–STPP–C-PC) were incorporated into gelatin-based systems and subjected to thermal treatment (25 °C or 100 °C for 15 min), before refrigerated storage for up to 22 days at 4 ± 2 °C (Fig. 6). Time points were selected based on safety guidelines for gelatin desserts (U.S. Department of Agriculture & U.S. FDA, 2024), with six days representing the typical shelf life and 22 days simulating extended storage.

Free C-PC exhibited a marked loss of its characteristic absorbance at λ 620 nm immediately after exposure to 100 °C, particularly in aqueous solution (Fig. 6). This thermal degradation was evident from day 0 and intensified during refrigerated storage, highlighting the intrinsic instability of free C-PC under conditions typically encountered in food processing and post-processing storage (Nowruzi et al., 2022). In contrast, the encapsulated formulations, CHT–C-PC [Fig. 6 **(B)**] and CHT–STPP–C-PC [Fig. 6 **(C)**], demonstrated notably greater spectral stability after heating, especially when incorporated into a gelatin matrix. Gelatin most probably contributed synergistically by forming a viscoelastic and semi-rigid network that limited the diffusion of oxygen and heat around the microparticles. Indeed, natural polymer hydrogels, including gelatin-based matrices, restrict molecular mobility and create diffusion barriers that enhance the structural and functional stability of proteins (Raza et al., 2018).

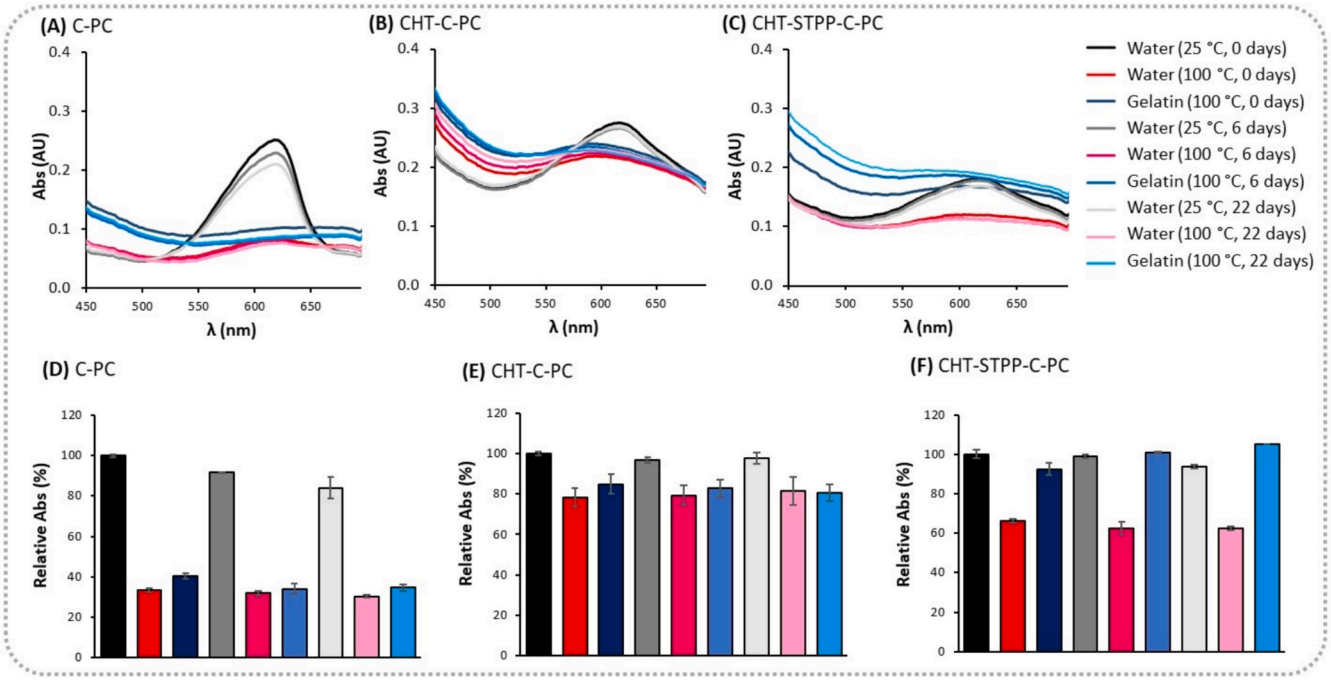

Fig. 6. Application of encapsulated C-PC as a gelatin dessert colorant. Absorbance spectra and relative Abs of (A, D) Free C-PC, (B, E) chitosan-C-phycocyanin (CHT–C-PC)-based microparticles, and (C, F) chitosan-STPP-C–phycocyanin (CHT–STPP–C-PC)-based microparticles (0.2 mg· mL^{-1} of C-PC) in MiliQ water or gelatin (24 mg· mL^{-1} of gelatin prepared with MiliQ water) after 15 min at 25 °C or 100 °C, followed by 0, 6, or 22 days of refrigeration at 4 °C with no light exposure. Abs of C-PC in water at 25 °C, 0 days, was the reference for 100 %.

The retention of absorbance even after heating and prolonged storage suggests that chitosan-based encapsulation, particularly with STPP crosslinking, provides effective protection against thermal degradation. These results demonstrate a protective effect of the encapsulation matrices, particularly the chitosan-based systems, which most likely act as physical barriers that reduce colorant degradation [89]. Additionally, these findings support that encapsulated C-PC formulations are promising natural colorants for thermally processed food products, combining visual appeal with improved functional stability.

4. Conclusion

Physicochemical and structural characterization confirmed the formation of a chitosan–C-PC polyelectrolyte hydrogel network, with microparticles exhibiting a mean diameter of ~3.8 μm, a positive ζ-potential above +24 mV, and an encapsulation efficiency exceeding 36 %. SAXS/USAXS analysis revealed a heterogeneous porous internal morphology, favoring effective C-PC entrapment and contributing to the functional integrity of the system. These structural features are key to the protective capacity of microparticles.

Encapsulation significantly enhanced C-PC stability under thermal stress, extreme pH conditions, and long-term light/dark storage by preserving absorbance and reducing turbidity. These improvements enabled the successful application of free C-PC as a natural blue colorant in gelatin-based desserts, where it exhibited rapid degradation. Encapsulated formulations-maintained color even after heating and refrigeration, indicating that they can be used in thermally processed foods with extended shelf life. Overall, spray-dried chitosan microparticles are a robust and scalable delivery system for stabilizing C-PC in food and other functional applications.

CRediT authorship contribution statement

Paulo Vitor França Lemos: Writing – review & editing, Writing – original draft, Validation, Methodology, Formal analysis, Data curation, Conceptualization. **Nathalia Vieira Porphirio Veríssimo:** Writing – review & editing, Writing – original draft, Validation, Methodology, Formal analysis, Data curation, Conceptualization. **Juliana Barone Teixeira:** Validation, Formal analysis, Data curation. **Henrique Rodrigues Marcelino:** Supervision, Resources, Project administration. **Guilherme Augusto Ferreira:** Supervision, Resources, Project administration. **Carolina Oliveira de Souza:** Supervision, Resources, Project administration. **Jania Betânia Alves da Silva:** Supervision, Resources, Project administration. **Thâmila Thalline Batista de Oliveira:** Formal analysis. **Cristiano Luis Pinto de Oliveira:** Validation, Formal analysis, Data curation. **Marcia Carvalho de Abreu Fantini:** Validation, Formal analysis, Data curation. **Valéria de Carvalho Santos-Ebinuma:** Supervision, Resources, Project administration.

Funding information

This study was financially supported by the Conselho Nacional de Desenvolvimento Científico e Tecnológico - CNPq (CNPq - 309955/2022–0 and INCT MIDAS CNPq - 465,594/2014–0), Coordenação de Aperfeiçoamento de Pessoal de Nível Superior - CAPES (CAPES PDPG - 88,881.708195/2022–01 and Finance Code 001, CAPES-Humboldt 20,240,026,595,432), Fundação de Amparo à Pesquisa do Estado da Bahia - FAPESB (INCITE PIE0006/2022), and Fundação de Amparo à Pesquisa do Estado de São Paulo – FAPESP (2021/06686–8, 2021/09175–4, 2022/14603–8, 2023/01368–3). Nathalia V. P. Veríssimo acknowledges support from FAPESP (grant no 2023/10479–3) and the PRPI – University of São Paulo ("Programa de Apoio a Novos Docentes (2024)", Process USP 22.1.09345.01.2). São Paulo Research Foundation – Brazil (FAPESP – Grant no 2021/06686–8). Valeria C. Santos-Ebinuma thanks CNPq (Proc. 306,475/2025–1). Juliana B. Teixeira thanks FAPESP for the scholarship (FAPESP – Grant no 2023/13069–0 and 2024/19904–1). Cristiano L. P. Oliveira CNPq grant number 307303/2023–3 and FAPESP grant number 2016/24531–3.

Declaration of competing interest

The authors declare that they have no known competing financial interests or personal relationships that could have appeared to influence the work reported in this paper.

Acknowledgements

The authors would like to dedicate this paper to Professor Dr. Janice Izabel Druzian (*in memorial*), who was always available to share her immeasurable knowledge with us at the Federal University of Bahia. We thank the CENTRAL DE ANÁLISES – UTFPR Campus Pato Branco (Universidade Tecnológica do Paraná – PR) for support in the SEM, XRD, DSC, and TG analysis.

This research used facilities of the Brazilian Synchrotron Light Laboratory (LNLS), part of the Brazilian Center for Research in Energy and Materials (CNPEM), a private non-profit organization under the supervision of the Brazilian Ministry for Science, Technology, and Innovations (MCTI). The Cateretê beamline staff is acknowledged for the assistance during the experiments 20241753.

Appendix A. Supplementary data

Supplementary data to this article can be found online at https://doi.org/10.1016/j.foodchem.2025.147358.

Data availability

Data will be made available on request.

References

Adjali, A., Clarot, I., Chen, Z., Marchioni, E., & Boudier, A. (2022). Physicochemical degradation of phycocyanin and means to improve its stability: A short review. *Journal of Pharmaceutical Analysis, 12*, 406–414. https://doi.org/10.1016/j.jpha.2021.12.005

Alhalaweh, A., Andersson, S., & Velaga, S. P. (2009). Dissolution rate enhancement of poorly water-soluble drugs through cocrystals: A case study of carbamazepine. *European Journal of Pharmaceutical Sciences, 38*, 206–213. https://doi.org/10.1016/j.ejps.2009.07.003

AnaSpec. (2025). C-Phycocyanin (AS-82003) – Product data sheet. Retrieved July 18, 2025, from https://www.eurogentec.com/assets/39016123-9e26-4d9e-830b-e33268c574f9/tds-en-as-82003-c-pc-c-phycocyanin.pdf.

Andreeva, D. V., Kollath, A., Brezhneva, N., Sviridov, D. V., Cafferty, B. J., Möhwald, H., & Skorb, E. V. (2017). Using a chitosan nanolayer as an efficient pH buffer to protect pH-sensitive supramolecular assemblies. *Physical Chemistry Chemical Physics, 19*, 23843–23848. https://doi.org/10.1039/C7CP02618H

Antonino, R. S. C. M. Q., Fook, B. R. P. L., Lima, V. A. O., Souza, R. M. C., Muniz, E. C., Beppu, M. M., et al. (2017). Preparation and characterization of chitosan obtained from shells of shrimp (*Litopenaeus vannamei*) by different deacetylation processes. *Marine Drugs, 15*, 141. https://doi.org/10.3390/md15050141

Aranaz, I., Paños, I., Peniche, C., Heras, Á., & Acosta, N. (2017). Chitosan spray-dried microparticles for controlled delivery of venlafaxine hydrochloride. *Molecules, 22*, 1980. https://doi.org/10.3390/molecules22111980

Azari, A., Mahdiuni, H., & Godehkahriz, S. (2023). Enhancement of thermal and pH stability of C-phycocyanin by microencapsulation using different biopolymers: A comparative study. *Algal Research, 72*, Article 103120. https://doi.org/10.1016/j.algal.2023.103120

Bai, Y., Li, X., Xie, Y., Wang, Y., Dong, X., & Qi, H. (2023). Ultrasound treatment enhanced the functional properties of phycocyanin with phlorotannin from *Ascophyllum nodosum*. *Frontiers in Nutrition, 10*, Article 1181262. https://doi.org/10.3389/fnut.2023.1181262

Bennett, A., & Bogorad, L. (1973). Complementary chromatic adaptation in a filamentous blue-green alga. *Journal of Cell Biology, 58*, 419–435. https://doi.org/10.1083/jcb.58.2.419

Böcker, L., Hostettler, T., Diener, M., Eder, S., Demuth, T., Adamcik, J., et al. (2020). Time–temperature-resolved functional and structural changes of phycocyanin extracted from *Arthrospira platensis* (*Spirulina*). *Food Chemistry, 316*, Article 126374. https://doi.org/10.1016/j.foodchem.2020.126374

Busto, M. D., González-Temiño, Y., & Pérez-Mateos, M. (2022). Microencapsulation of a commercial food-grade protease by spray-drying in chitosan/TPP matrices. *Foods, 11*, 2077. https://doi.org/10.3390/foods11142077

Cervera, M. F., Heinämäki, J., Paz, N., Horna, O., Holm, P., & Juppo, A. M. (2011). Design and characterization of chitosan-based coated matrix tablets. *AAPS PharmSciTech, 12*, 637–649. https://doi.org/10.1208/s12249-011-9620-3

Chaiklahan, P., Chirasuwan, N., & Bunnag, B. (2021). Stability of phycocyanin extracted from *Spirulina* sp.: Influence of temperature, pH and preservatives. *Algal Research, 58*, Article 102391. https://doi.org/10.1016/j.algal.2021.102391

Chamorro-Cevallos, G., Barrón, B. L., García, J. L., Madrigal-Bujaidar, E., Cruz-Vega, D. E., Pages, N., et al. (2020). Phycocyanin: A potential therapeutic agent against cardiovascular disease. *Life Sciences, 261*, Article 118470. https://doi.org/10.1016/j.lfs.2020.118470

Cheng, Z., Zhang, W., Hou, X., Wang, B., Zhu, Y., Zhang, P., et al. (2019). Synthesis, characterization, and evaluation of redox-sensitive chitosan oligosaccharide nanoparticles coated with *phycocyanin* for drug delivery. *Nanoscale Research Letters, 14*, 389. https://doi.org/10.1186/s11671-019-3207-4

Desai, K. G. H., & Park, H. J. (2005a). Recent developments in microencapsulation of food ingredients. *Drug Development Research, 64*, 114–125. https://doi.org/10.1002/ddr.10416

Desai, K. G. H., & Park, H. J. (2005b). Recent trends in microencapsulation of food ingredients using biopolymer-based delivery systems. *Journal of Microencapsulation, 22*, 377–395. https://doi.org/10.1080/02652040500100139

DIC Corporation. (2016). DIC announces major expansion of production capacity for Linablue® natural blue food coloring Accessed April 2025 from https://www.dic-global.com/en/news/2016/ir/20161116000010.html.

Downham, A., & Collins, P. (2000). Colouring our foods in the last and next millennium. *International Journal of Food Science & Technology, 35*, 5–22. https://doi.org/10.1046/j.1365-2621.2000.00373.x

Eriksen, N. T. (2008). Production of phycocyanin — A pigment with applications in biology, biotechnology, foods and medicine. *Applied Microbiology and Biotechnology, 80*, 1–14. https://doi.org/10.1007/s00253-008-1542-y

Esatbeyoglu, T., Hardt, D. J., Buerk, J. R., Schlösser, F. P., & Rimbach, J. L. (2017). Stability, bioavailability and antioxidant capacity of phycocyanin. *Nutrients, 9*, 1313. https://doi.org/10.3390/nu9121313

Frank, G., Richter, H., Stetzler, H., & Jaenicke, R. (1978). The complete amino acid sequence of both subunits of C-phycocyanin from the cyanobacterium *Mastigocladus laminosus*. *Hoppe-Seyler's Zeitschrift für Physiologische Chemie, 359*, 1651–1661.

Galasso, C., Corinaldesi, C., & Sansone, C. (2019). A comparative study of the antioxidant, anti-inflammatory and cytotoxic properties of marine algal extracts. *Nutrients, 11*, 1226. https://doi.org/10.3390/nu11061226

Galván, K. L. P., Veríssimo, N. V. P., Santana, J. S., Silva, E. J., Oliveira, F. C., Druzian, J. I., et al. (2024). Encapsulation of polyketide colorants in chitosan and maltodextrin microparticles. *International Journal of Biological Macromolecules, 269*, Article 132173. https://doi.org/10.1016/j.ijbiomac.2024.132173

Gieroba, B., Sroka-Bartnicka, A., Kazimierczak, P., Kalisz, G., Maciejewska, B., Wiater, A., et al. (2022). Structural and physicochemical characterization of natural polysaccharides from selected medicinal plants. *International Journal of Molecular Sciences, 23*, 5953. https://doi.org/10.3390/ijms23115953

Giroux, H. J., Lanouette, G., & Britten, M. (2015). Controlled release of bioactive compounds from gelled double emulsions stabilized by whey protein isolate. *Food Hydrocolloids, 45*, 272–279. https://doi.org/10.1016/j.foodhyd.2014.12.004

Glatter, O. (1977). A new method for the evaluation of small-angle scattering data. *Journal of Applied Crystallography, 10*, 415–421. https://doi.org/10.1107/S0021889877015879

GNT Group. (2019). Improved heat stability of natural blue colorants. Retrieved April 2025 from https://exberry.com/en/color-insights/improved-heat-stability-of-natural-blue-colorants/.

Grand View Research. (2023). Phycocyanin market size to reach $276.4 million by 2030. Retrieved April 2025 from https://www.grandviewresearch.com/press-release/global-phycocyanin-market.

Gustiningtyas, A., Pertiwi, S., Nurdjanah, S., & Anggraeni, R. (2020). Microencapsulation of C-phycocyanin from *Spirulina platensis* using sodium alginate–maltodextrin matrix through spray drying. *IOP Conference Series: Earth and Environmental Science, 414*, Article 012005. https://doi.org/10.1088/1755-1315/414/1/012005

Harrick, N. J. (1967). *Internal reflection spectroscopy*. New York, NY: Wiley.

Helbling, I. M., Busatto, C. A., Fioramonti, S. A., Ruiz, M. E., Estenoz, D. A., Luna, J. A., et al. (2018). Chitosan microparticles produced by spray drying as a promising carrier for the oral delivery of insulin. *Pharmaceutical Research, 35*, 66. https://doi.org/10.1007/s11095-018-2363-z

IMB Jena Image Library. (2025). *Determination of secondary structure in proteins by FTIR spectroscopy*. Jena, Germany: Leibniz Institute on Aging – Fritz Lipmann Institute (FLI). Retrieved from https://www.leibniz-fli.de.

Jiang, L., Wang, Y., Yin, Q., Liu, G., Liu, H., Huang, Y., & Li, B. (2017). Phycocyanin: A potential drug for cancer treatment. *Journal of Cancer, 8*, 3416–3429. https://doi.org/10.7150/jca.21058

Kašpar, O., Jakubec, M., & Štěpánek, F. (2013). Characterization of spray-dried chitosan–TPP microparticles formed by two- and three-fluid nozzles. *Powder Technology, 240*, 31–40. https://doi.org/10.1016/j.powtec.2012.07.010

Katsarov, P. D., Pilicheva, B. A., Manev, H. M., Lukova, P. K., & Kassarova, M. I. (2017). Optimization of chitosan microspheres spray drying via 3^2 full factorial design. *Folia Medica, 59*, 310–317. https://doi.org/10.1515/folmed-2017-0037

Kotlarchyk, M., & Chen, S. H. (1983). Analysis of small-angle scattering spectra from polydisperse interacting colloids. *Journal of Chemical Physics, 79*, 2461–2469. https://doi.org/10.1063/1.445002

Koyande, A. K., Chew, K. W., Rambabu, K., Tao, Y., Chu, D. T., & Show, P. L. (2019). Microalgae: A potential alternative to health supplementation for humans. *Food Science and Human Wellness, 8*, 16–24. https://doi.org/10.1016/j.fshw.2019.03.001

Kusonwiriyawong, C., Lipipun, V., Vardhanabhuti, N., Zhang, Q., & Ritthidej, G. C. (2013). Spray-dried chitosan microparticles for cellular delivery of an antigenic protein: Physico-chemical properties and cellular uptake by dendritic cells and macrophages. *Pharmaceutical Research, 30*, 1677–1697. https://doi.org/10.1007/s11095-013-1014-7

Lauceri, R., Zittelli, G. C., & Torzillo, G. (2019). A simple method for rapid purification of phycobiliproteins from *Arthrospira platensis* and *Porphyridium cruentum* biomass. *Algal Research, 44*, Article 101685. https://doi.org/10.1016/j.algal.2019.101685

Lemos, P. V. F., Opretzka, L. C. F., Almeida, L. S., Cardoso, L. G., Silva, J. B. A., Souza, C. O., et al. (2020). Preparation and characterization of C-phycocyanin coated with STMP/STPP cross-linked starches from different botanical sources. *International Journal of Biological Macromolecules, 159*, 739–750. https://doi.org/10.1016/j.ijbiomac.2020.05.111

Loh, N.-T. D., & Elser, V. (2009). Reconstruction algorithm for single-particle diffraction imaging experiments. *Physical Review E, 80*, Article 026705. https://doi.org/10.1103/physreve.80.026705

Machado, S. S. N., Silva, J. B. A., Nascimento, R. Q., Souza, C. O., Cardoso, L. G., Druzian, J. I., et al. (2024). Insect residues as an alternative and promising source for the extraction of chitin and chitosan. *International Journal of Biological Macromolecules, 254*, Article 127773. https://doi.org/10.1016/j.ijbiomac.2023.127773

Martelli, G., Folli, C., Visai, L., Daglia, M., & Ferrari, D. (2014). Thermal stability improvement of blue colorant C-phycocyanin from *Spirulina platensis* for food industry applications. *Process Biochemistry, 49*, 154–159. https://doi.org/10.1016/j.procbio.2013.10.008

Meng, Q., Zhong, S., Wang, J., Li, X., Zhao, Y., Chen, H., et al. (2023). Chitosan-based microparticles for controlled release: Design, development and applications in food and pharmaceuticals. *Carbohydrate Polymers, 300*, Article 120265. https://doi.org/10.1016/j.carbpol.2022.120265

Mezzenga, R., & Fischer, P. (2013). The self-assembly, aggregation and phase transitions of food protein systems in one, two and three dimensions. *Reports on Progress in Physics, 76*, Article 046601. https://doi.org/10.1088/0034-4885/76/4/046601

Milenkova, S., Ambrus, R., Mukhtar, M., Szabó-Révész, P., Gurikov, P., Smirnova, I., et al. (2024). Development and evaluation of spray-dried chitosan microparticles containing voriconazole for pulmonary delivery. *Gels, 10*, 189. https://doi.org/10.3390/gels10030189

Mitra, S., Siddiqui, W. A., & Khandelwal, S. (2015). C-phycocyanin modulates sodium arsenite-induced oxidative stress and genotoxicity in mice. *Chemico-Biological Interactions, 238*, 138–147. https://doi.org/10.1016/j.cbi.2015.06.016

Moraes, C. C., Sala, T. N., & Costa, J. A. (2020). C-phycocyanin extraction from *Spirulina platensis* wet biomass using recyclable ionic liquid-based aqueous two-phase system. *Process Biochemistry, 94*, 317–324. https://doi.org/10.1016/j.procbio.2020.04.027

Naturex, S. A. (2025). Naturex SA – PatSnap Discovery. Retrieved April 2025, from https://discovery.patsnap.com/company/naturex-sa/.

Nowruzi, B., Konur, O., & Anvar, S. A. A. (2022). The stability of the phycobiliproteins in the adverse environmental conditions relevant to the food storage. *Food and Bioprocess Technology, 15*, 2646–2663. https://doi.org/10.1007/s11947-022-02855-8

Olas, B., Białecki, J., Urbańska, K., & Bryś, M. (2021). The effects of natural and synthetic blue dyes on human health: A review of current knowledge and therapeutic perspectives. *Advances in Nutrition, 12*, 2301–2311. https://doi.org/10.1093/advances/nmab081

Oliveira, C. L. P. (2011). Small-angle X-ray scattering and the study of nanostructures. In D. A. Chandrasekaran (Ed.), *Current trends in X-ray crystallography* (pp. 367–392). InTech.

Oliveira, C. L. P. (2016). *Modelagem de dados de espalhamento e difração a baixos ângulos* [Doctoral thesis, University of São Paulo]. Retrieved from https://teses.usp.br/teses/disponiveis/livredocencia/43/tde-04032016-175643/publico//Livre_Docencia_crislpo_revisado.pdf.

Oliveira, C. L. P., Behrens, M. A., Pedersen, J. S., Erlacher, K., Foss, M., Otzen, D. E., et al. (2009). A SAXS study of glucagon fibrillation. *Journal of Molecular Biology, 387*, 147–161. https://doi.org/10.1016/j.jmb.2009.01.020

Özkan, G., & Bilek, S. E. (2014). Microencapsulation of natural food colourants. *International Journal of Nutrition and Food Sciences, 3*, 162–169. https://doi.org/10.11648/j.ijnfs.20140303.13

Paluszkiewicz, C., Wesełucha-Birczyńska, A., Stodolak-Zych, E., Blazewicz, M., Pięt, A., Sitarz, M., et al. (2011). Spectroscopic study of chitosan and chitosan complexes with sodium hyaluronate and heparin. *Vibrational Spectroscopy, 60*, 185–192. https://doi.org/10.1016/j.vibspec.2011.12.004

Parshina, E. Y., Liu, W., Yusipovich, A. I., Chukhutsina, V. U., Ruban, A. V., Gorbunov, M. Y., et al. (2024). Spectral and conformational characteristics of phycocyanin associated with changes of medium pH. *Photosynthesis Research, 161*, 93–103. https://doi.org/10.1007/s11120-023-01068-0

Patel, A., Mishra, S., Pawar, R., & Ghosh, P. K. (2005). Purification and characterization of C-phycocyanin from cyanobacterial species of marine and freshwater habitat. *Protein Expression and Purification, 40*, 248–255. https://doi.org/10.1016/j.pep.2004.10.028

Pathare, P. B., Opara, U. L., & Al-Said, F. A. J. (2013). Colour measurement and analysis in fresh and processed foods: A review. *Food and Bioprocess Technology, 6*, 36–60. https://doi.org/10.1007/s11947-012-0867-9

Patil, G., Chethana, R., Sridevi, H. S., & Raghavarao, R. (2006). Purification of C-phycocyanin by two-step process. *Journal of Chromatography A, 1127*, 76–81. https://doi.org/10.1016/j.chroma.2006.05.073

Payne, E. J. R., Griffiths, M., Harrison, S. T. L., & Fagan-Endres, M. A. (2025). Exploring the activated charcoal adsorption column to improve cosmetic grade C-phycocyanin

purification from *Spirulina*. *Journal of Applied Phycology, 37*, 885–897. https://doi.org/10.1007/s10811-025-03458-4

Pedersen, J. S. (1997). Analysis of small-angle scattering data from colloids and polymer solutions: Modeling and least-squares fitting. *Advances in Colloid and Interface Science, 70*, 171–210. https://doi.org/10.1016/S0001-8686(97)00312-6

Pinto, L. (2011). Investigating macromolecular complexes in solution by small angle X-ray scattering. *InTechOpen*. https://doi.org/10.5772/30730

Prashanth, K. K. H., Kittur, F. S., & Tharanathan, R. N. (2002). Solid state structure of chitosan prepared under different N-deacetylating conditions. *Carbohydrate Polymers, 50*, 27–33. https://doi.org/10.1016/S0144-8617(01)00371-X

Queiroz, M. F. F., Melo, K. R. T., Sabry, D. A., Sassaki, G. L., & Rocha, H. A. O. (2014). Does the use of chitosan contribute to oxalate kidney stone formation? *Marine Drugs, 13*, 141–158. https://doi.org/10.3390/md13010141

Rasmussen, M. K., Bordallo, H. N., Bordenalli, M. A., Akamatsu, M. A., Trezena, A. G., Tino-De-Franco, M., et al. (2021). Assessing the efficiency of SBA-15 as a nanocarrier for diphtheria anatoxin. *Microporous and Mesoporous Materials, 312*, Article 110763. https://doi.org/10.1016/j.micromeso.2020.110763

Raza, F., Zafar, H., Zhu, Y., Ren, Y., Ullah, A., Khan, A. U., et al. (2018). A review on recent advances in stabilizing peptides/proteins upon fabrication in hydrogels from biodegradable polymers. *Pharmaceutics, 10*(1), 16. https://doi.org/10.3390/pharmaceutics10010016

Reddy, C. M., & Subhashini, S. B. (2000). C-phycocyanin inhibits reactive oxygen species formation and DNA strand breaks in human lymphocytes. *Biochemical and Biophysical Research Communications, 277*, 599–603. https://doi.org/10.1006/bbrc.2000.3715

Rouquerol, J., Llewellyn, P., & Rouquerol, F. (2014). *Adsorption by powders and porous solids* (2nd ed.). Academic Press.

Santos, N. V. D., Saponi, C. F., Greaves, T. L., & Pereira, J. F. B. (2019). Revealing a new fluorescence peak of the enhanced green fluorescent protein using three-dimensional fluorescence spectroscopy. *RSC Advances, 9*, 22853–22858. https://doi.org/10.1039/C9RA02567G

Schneider, C. A., Rasband, W. S., & Eliceiri, K. W. (2012). NIH image to ImageJ: 25 years of image analysis. *Nature Methods, 9*, 671–675. https://doi.org/10.1038/nmeth.2089

Scientific Laboratory Supplies. (2023). Low MW chitosan (Sigma-Aldrich). Retrieved February 21, 2024, from https://www.scientificlabs.ie/product/448869-50G.

Sechi, N. S. M., & Marques, P. T. (2017). Preparation and physicochemical, structural and morphological characterization of phosphorylated starch. *Materials Research, 20*, 174–180. https://doi.org/10.1590/1980-5373-MR-2016-1008

Sensient Technologies. (2025). Sensient Technologies Corporation. Retrieved April 2025, from https://www.sensient.com/.

Sergeeva, Y. E., Demina, N. B., & Sergeev, V. V. (2023). Microencapsulation of natural blue pigment C-phycocyanin: Stability improvement and delivery strategies. *Biotechnology, 12*, 55. https://doi.org/10.3390/biotech12030055

Sergeeva, Y. E., Zakharevich, A. A., Sukhinov, D. V., Koshkalda, A. I., Kryukova, M. V., Malakhov, S. N., et al. (2023). Chitosan sponges for efficient accumulation and controlled release of C-phycocyanin. *Biotech, 12*, 55. https://doi.org/10.3390/biotech12030055

Sevenou, O., Hill, S., Farhat, I. A., & Mitchell, J. R. (2002). Organisation of the external region of the starch granule as determined by infrared spectroscopy. *International Journal of Biological Macromolecules, 31*, 79–85. https://doi.org/10.1016/S0141-8130(02)00067-3

Seyed Yagoubi, A., Shahidi, F., Mohebbi, M., & Varidi, M. (2018). Preparation, characterization and evaluation of physicochemical properties of phycocyanin-loaded solid lipid nanoparticles and nanostructured lipid carriers. *Food Measurement and Characterization, 12*, 378–385. https://doi.org/10.1007/s11694-017-9650-y

Shih, C.-M., Cheng, S.-N., & Wong, C.-S. (2009). Antinociceptive effect of C-phycocyanin on mice treated with lipopolysaccharide. *Anesthesia & Analgesia, 108*, 1303–1310. https://doi.org/10.1213/ane.0b013e3181964e6f

Sigurdson, G. T., Tang, P. M., & Giusti, M. M. (2017). Natural colorants: Food colorants from natural sources. *Annual Review of Food Science and Technology, 8*, 261–280. https://doi.org/10.1146/annurev-food-030216-025923

Soni, R., Sudhakar, K., & Rana, R. S. (2020). A review on encapsulation of natural colors: Stability and delivery mechanisms. *International Journal of Biological Macromolecules, 157*, 240–252. https://doi.org/10.1016/j.ijbiomac.2020.04.182

Svergun, D. I., & Koch, M. H. J. (2003). Small-angle scattering studies of biological macromolecules in solution. *Reports on Progress in Physics, 66*, 1735–1782. https://doi.org/10.1088/0034-4885/66/10/R05

Tansi, F. L., Rüger, R., Rabenhold, M., Steiniger, F., Fahr, A., & Hilger, I. (2015). Fluorescence-quenching of a liposomal-encapsulated near-infrared fluorophore as a tool for *in vivo* optical imaging. *Journal of Visualized Experiments, 95*, Article 52136. https://doi.org/10.3791/52136

Teixeira, J. A. (1988). Small-angle scattering by fractal systems. *Journal of Applied Crystallography, 21*, 781–785. https://doi.org/10.1107/S0021889888000263

Thommes, M., Kaneko, K., Neimark, A. V., Olivier, J. P., Rodriguez-Reinoso, F., Rouquerol, J., et al. (2015). Physisorption of gases, with special reference to the evaluation of surface area and pore size distribution (IUPAC technical report). *Pure and Applied Chemistry, 87*, 1051–1069. https://doi.org/10.1515/pac-2014-1117

U.S. Department of Agriculture & U.S. Food and Drug Administration. (2024). FoodKeeper app – Keep food safe. FoodSafety.gov. Retrieved July 18, 2025, from https://www.foodsafety.gov/keep-food-safe/foodkeeper-app.

U.S. Food and Drug Administration (FDA). (2012). Agency response letter GRAS Notice No. GRN 000424: *Phycocyanin* from *Arthrospira platensis*. Retrieved July 18, 2025, from https://www.fda.gov/media/80699/download.

U.S. Food and Drug Administration (FDA). (2024). HHS, FDA to phase out petroleum-based synthetic dyes from nation's food supply. Press announcement. Retrieved July 18, 2025, from https://www.fda.gov/news-events/press-announcements/hhs-fda-phase-out-petroleum-based-synthetic-dyes-nations-food-supply.

Veríssimo, N. V., Nakamura, C. N., de Oliveira, F., Kuhn, B. L., Frizzo, C. P., Pereira, J. F., et al. (2022). Effect of amphiphilic ionic liquids on the colorimetric properties of polyketide colorants. *Journal of Molecular Liquids, 363*, Article 119857. https://doi.org/10.1016/j.molliq.2022.119857

Wang, X., Xie, Y., Zhou, Z., Ruan, R., Zhou, C., & Cheng, Y. (2025). Factors influencing phycocyanin synthesis in microalgae and culture strategies: Toward efficient production of alternative proteins. *Sustainability, 17*, 5962. https://doi.org/10.3390/su17135962

Wongsagonsup, R., Shobsngob, S., Oonkhanond, B., & Varavinit, S. (2005). Zeta potential (ζ) and pasting properties of phosphorylated or cross-linked rice starches. *Starch/Stärke, 57*, 32–37. https://doi.org/10.1002/star.200400311

Yuan, B., Chen, X., Li, X., Dong, C., & Feng, Y. (2022). A review of recent strategies to improve the physical stability of phycocyanin. *Current Research in Food Science, 5*, 2329–2337. https://doi.org/10.1016/j.crfs.2022.11.033

Zhang, J., Liu, D., Cao, Y., Zhang, Y., & Chen, J. (2022). Stabilization of C-phycocyanin by spray-drying using different combinations of wall materials. *Food Chemistry, 372*, Article 131242. https://doi.org/10.1016/j.foodchem.2021.131242

Zhang, X., Wei, L., & Smith, J. (2021). Thermal degradation and stabilization mechanism of chitosan-based films: Effect of molecular weight and plasticizer. *Polymer Degradation and Stability, 190*, Article 109550. https://doi.org/10.1016/j.polymdegradstab. 2021.109550

Zhang, Y., Zhang, Z., Chen, X., Wang, X., Liu, C., Xu, Y., et al. (2023). Ultrasound-assisted encapsulation of C-phycocyanin into multilayered liposomes: Stability and antioxidant activity. *Food Chemistry, 423*, Article 136274. https://doi.org/10.1016/j.foodchem.2023.136274